ChemComm
Chemical Communications

Accepted Manuscript

This article can be cited before page numbers have been issued, to do this please use: Y. Kita, M. Takeuchi and Y. Amao, *Chem. Commun.*, 2026, DOI: 10.1039/D6CC00317F.

ROYAL SOCIETY OF CHEMISTRY

rsc.li/chemcomm

View Article Online
DOI: 10.1039/D6CC00317F

Journal Name

Review

CO_2-based biodegradable plastic and its precursor production using photo-biocatalytic processes

Received 00th January 20xx,
Accepted 00th January 20xx

DOI: 10.1039/x0xx00000x

www.rsc.org/

Yu Kita [a], Mika Takeuchi [b] and Y. Amao[a,b,c*]

Biodegradable plastics are materials that can be decomposed by the action of microbes into water, CO_2, and biomass. Biodegradable plastics are attractive materials to solve serious environmental pollution due to plastic disposal. Some biodegradable plastics are produced entirely from petroleum-based precursors. A new biodegradable plastics and their precursors production from CO_2 and persistency organic or bio-based compound using a visible-light driven redox with biocatalytic processes is one of the effective resolutions for environmental issues both plastic pollution and global warming. In this review article, recent research on the visible-light driven production of CO_2-based biodegradable plastics and their precursors with the system of light-driven redox and biocatalytic processes is introduced. As a first example, an overview of research into the production of biodegradable plastics, poly(hydroxybutyrate) (PHB) and their precursors such as acetate, shikimic acid, acetoin and so on from CO_2 using semiconductor photocatalyst-based photoredox system with microbial cell as a biocatalytic process is provided. As a second example, an overview of studies on the production of biodegradable plastic precursors, 3-hydroxybutyrate, L-malate and fumarate from CO_2 and small organic molecules using organic dye-based photoredox system with an electron donor, an electron mediator and enzyme-based biocatalytic processes is provided.

Introduction

Plastic is a versatile, lightweight, and relatively inexpensive material that has been an indispensable part of modern life.[1] Most plastics continue to be made from fossil resources, primarily petroleum, and the manufacturing process leads to increasing greenhouse gas emissions throughout the value chain.[2] Plastics pose environmental pollution concerns throughout their entire life cycle, from production to use and ultimately disposal.[3,4] However, plastics have a wide range of functions and are useful materials that support modern society, so it is necessary to establish methods for their production, use, and disposal without causing environmental pollution.[5] In view of these social conditions, biodegradable plastics are attracting attention as a material to replace conventional plastics.[6-12] Biodegradable and its derivative materials are broken down by microbes into water and CO_2 mainly over a period of time.[13-17] Among the various biodegradable plastics, aliphatic polyester-based biodegradable plastics include poly(lactic acid) (PLA),[18-21] poly(hydroxyalkanoate) (PHA),[22-31] poly(glycolic acid) (PGA),[32-35] poly(caprolactone) (PCL),[36-40] poly(butylene succinate) (PBS)[41-44], poly(carbonate)[45-49] and so on as shown in Figure 1.

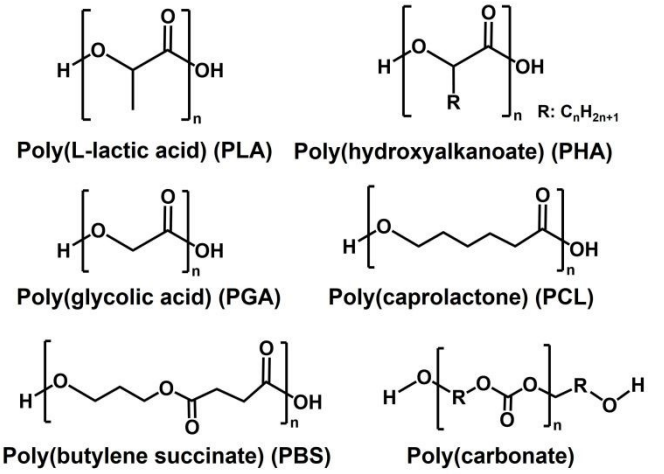

Fig. 1. Chemical structures of typical biodegradable plastics

These biodegradable plastic precursors are synthesised from various molecules, such as biological and petroleum-derived. Therefore, precursors are synthesised using petroleum-derived material, and it is required to establish the precursors synthesis method from renewable raw materials such as CO_2 and biomass derived molecules in the future. In natural photosynthesis, visible light energy is used as the driving force to produce glucose, starch, and oxygen using CO_2 and water as raw materials.[50-55] Thus, natural photosynthetic processes can serve as a model for CO_2-based synthesis of polymers and their

[a] Graduate School of Science, Osaka City University, Sugimoto 3-3-138, Sumiyoshi-ku, Osaka 558-8585, Japan
[b] Graduate School of Science, Osaka Metropolitan University, Sugimoto 3-3-138, Sumiyoshi-ku, Osaka 558-8585, Japan
[c] Research Centre for Artificial Photosynthesis, Osaka Metropolitan University, Sugimoto 3-3-138, Sumiyoshi-ku, Osaka 558-8585, Japan
E-mail: amao@omu.ac.jp

DOI: 10.1039/x0xx00000x

View Article Online
DOI: 10.1039/D6CC00317F

precursors. Natural photosynthesis consists of a light-dependent reactions and a dark reactions. The main components involved in the light-dependent reactions are the photosystem, the complexes that capture light energy, chlorophylls, the main light-absorbing pigments, the electron transport chain that transports electrons and contributes to the production of adenosine triphosphate (ATP) and nicotinamide adenine dinucleotide phosphate reduced form (NADPH), ATP synthase and ferredoxin NADP$^+$ reductase. In summary, the light-dependent reactions are the process of absorbing visible-light energy and using that energy to convert it into the ATP and NADPH.

The dark reactions, collectively known as the Calvin cycle,[56,57] do not directly require visible-light energy but utilize the ATP and NADPH produced during the light-dependent reactions to fix CO_2 into organic compound such as ribulose-1,5-bisphosphate and convert it into glucose with some enzymatic processes. Biodegradable plastics and their precursors are synthesized starting from compounds synthesized from CO_2 produced in the Calvin cycle using microalgae. It has been reported that D-lactate, a precursor for poly(lactic acid), was produced using malic enzyme (ME)-overexpressing strains of cyanobacterium *Synechocystis* sp. PCC6803 as shown in Figure 2.[58]

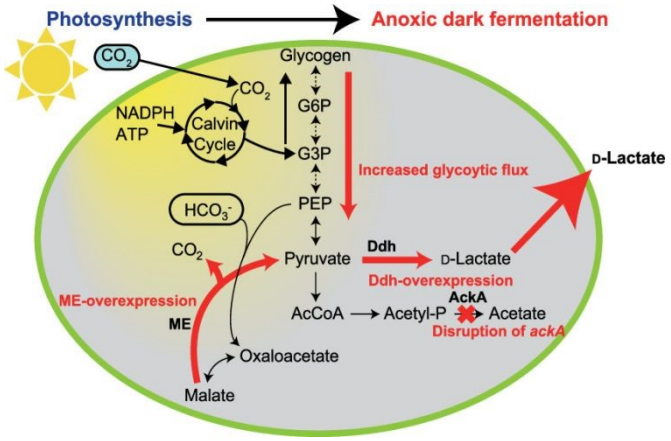

Fig. 2. Light-driven D-lactate production from CO_2 using *Synechocystis* sp. PCC6803. G6P: glucose-6-phosphate, G3P: glyceraldehyde 3-phosphate, PEP: phosphoenolpyruvic acid, ME: malic enzyme, Ddh: D-lactate dehydrogenase, AckA: acetate kinase A. Reproduced with permission from ref 58. Copyright 2020 American Chemical Society.

A metabolic map of the TCA cycle in *Synechocystis* sp. PCC 6803 is shown in Figure 3.[59] As shown in Figure 3, not only D-lactate but also various biodegradable plastic precursors such as succinate, 3-hydroxybutyrate, and 3-hydroxypropionate can be produced from CO_2 under visible-light irradiation using *Synechocystis* sp. PCC 6803. Also, poly(hydroxybutyrate) (PHB) is produced from CO_2 using *Synechocystis* sp. PCC 6803. The metabolic map in Figure 3 shows that the production of acetyl Co-A from CO_2 leads to the production of various biodegradable plastic precursors. It will also be possible to produce biodegradable plastic precursors such as fumarate and malate.

In this way, by linking the TCA cycle and glycolysis with the photosynthetic process, it is possible to synthesize biodegradable plastics and their precursors from CO_2 driven by light energy.

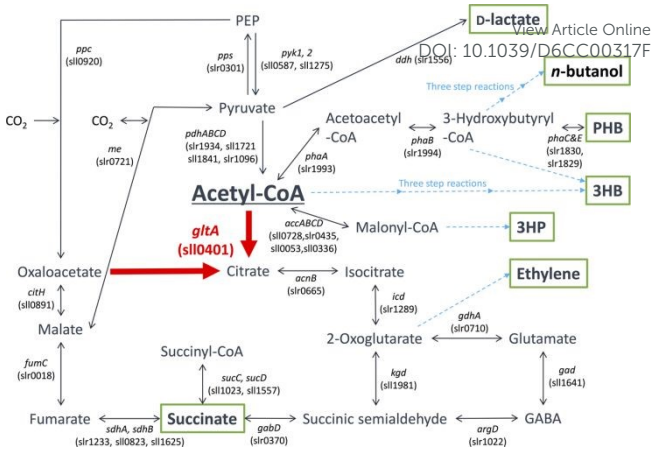

Fig. 3. Metabolic map in the TCA cycle in *Synechocystis* sp. PCC 6803. *accABCD*: acetyl-CoA carboxylase, *acnB*: aconitase, *argD*: D-arginine dehydrogenase, *citH*, malate dehydrogenase, *ddh*: D-lactate dehydrogenase, *fumC*: fumarase, *gabD*: succinate-semialdehyde dehydrogenase, *gad*: glutamate decarboxylase, *gdhA*: glutamate dehydrogenase, *gltA*: citrate synthase, *icd*: isocitrate dehydrogenase, *kgd*: 2-oxoglutarate decarboxylase, *me*: malic enzyme, *pdh*ABCD: pyruvate dehydrogenase, *phaA*: β-ketothiolase, *phaB*: acetoacetyl-CoA reductase, *phaC&E*: polyhydroxyalkane synthase, *ppc*: phosphoenolpyruvate carboxylase, *pps*: phosphoenolpyruvate synthase, *pyk1, 2*: pyruvate kinase, *sdhA, sdhB*: succinate dehydrogenase, *sucC, sucD*: succinate dehydrogenase. A. Reproduced with permission from ref 59. Copyright 2019 The authors Creative Commons CC-BY-NC-ND license.

To develop a visible-light driven production of CO_2-based biodegradable plastic and its precursor based on the mechanisms of natural photosynthesis and microalgae, a method of linking light-driven redox (light-dependent reaction) with reactions mediated by biocatalytic processes such as microbials or enzymes (dark reaction), as shown in Figure 4.

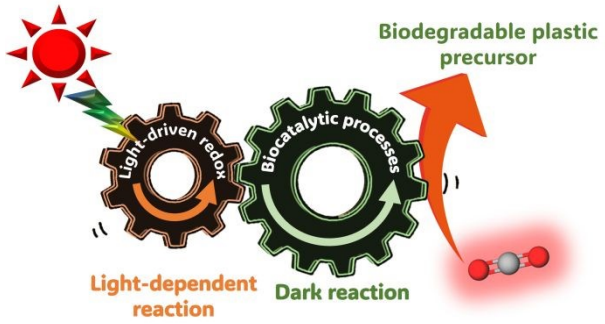

Fig. 4. CO_2-based biodegradable plastic and its precursor production with the system of visible-light driven redox and biocatalytic processes.

By using semiconductor photocatalysts and organic dyes in the light-driven redox system, the light-harvesting and sensitizing functions can be enhanced compared to natural photosynthesis such as in microalgae. Biocatalytic processes use microorganisms directly or through cascades of enzymes to produce biodegradable plastics and their precursors from CO_2. By linking these two processes, it is expected that biodegradable plastics and their precursors can be produced by fixing CO_2 to organic molecules using visible-light energy as a driving force.

In this revies article, recent research on the visible-light driven production of CO_2-based biodegradable plastics and their precursors with the system of light-driven redox and biocatalytic processes is introduced. First, research on the production of biodegradable plastics and their precursors using semiconductor photocatalysts as photoredox and microbials as biocatalytic processes will be introduced. Second, research on

the production of biodegradable plastic precursors using organic dye-based photoredox and enzyme-based biocatalytic processes will be introduced.

Strategy for visible-light driven production of CO_2-based biodegradable plastics and their precursors with photocatalyst and microbial cells hybrid system

Semiconductor-based photocatalysts are highly efficient at capturing and converting solar energy compared to the light-harvesting function of natural photosynthesis. Meanwhile, natural CO_2 fixation, primarily by plants and microorganisms, is the basis for life and biological processes. By directly contacting semiconductor-based photocatalysts with microbial cells expressing a CO_2 fixation pathway as shown in Figure 5(a), light-driven biodegradable plastics and their precursors can be produced. Also, the system for biodegradable plastics and their precursors production from CO_2 using the microbial cells and extract containing enzymes as the biocatalyst in a visible light-driven redox system consisting of an electron donor (ED), a visible light sensitizer (PS), and an electron mediator (EM) have also proposed as shown in Figure 5(b).

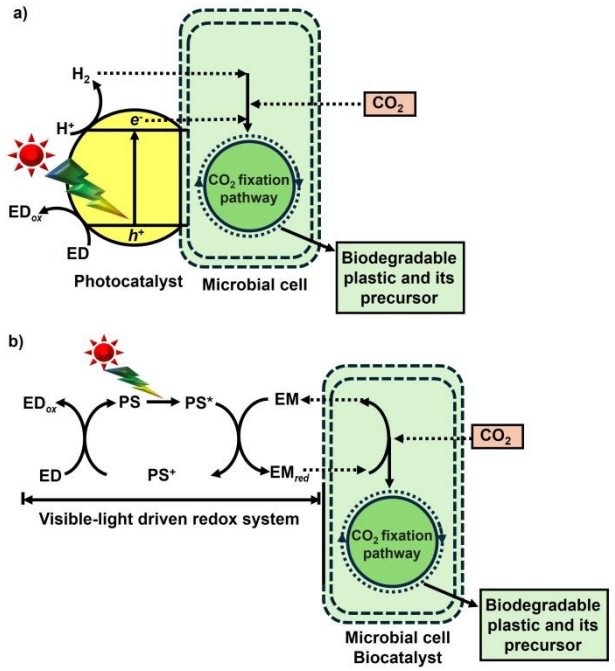

Fig. 5. Visible-light driven biodegradable plastic and its precursor production based on the CO_2 fixation using photocatalyst and microbial cell hybrid system (a) and hybrid system of photoredox consisting of an electron donor (ED), a visible light sensitizer (PS), and an electron mediator (EM) and the microbial cells or biocatalysts (b).

In the system as shown Figures 5(a) and (b), a visible light responsive photocatalyst capable of decomposing water into oxygen and hydrogen is used.[60-65] On the other hand, the CO_2 fixation pathway within microbial cells for the production of biodegradable plastics and their precursors is shown in Figure 6. As shown in Figure 6, natural CO_2 fixation pathways are classified into the following six categories: Calvin Benson Bassham (CBB) cycle,[66] 3-hydroxypropionate pathway,[67] reductive acetyl-CoA (Wood-Lijungdah (WL) pathway) pathway,[68] reductive TCA cycle,[69] dicarboxylate/4-hydroxybutyrate cycle,[70] and 3-hydroxypropionate/4-hydroxybutyrate cycle.[71] In particular, the reductive acetyl-CoA pathway, known as the Wood-Ljungdah (WL) pathway, is expressed in *Moorella thermoacetica* (*M. thermoacetica*) and is used to produce acetate from CO_2[72-75] in combination with a photocatalyst.

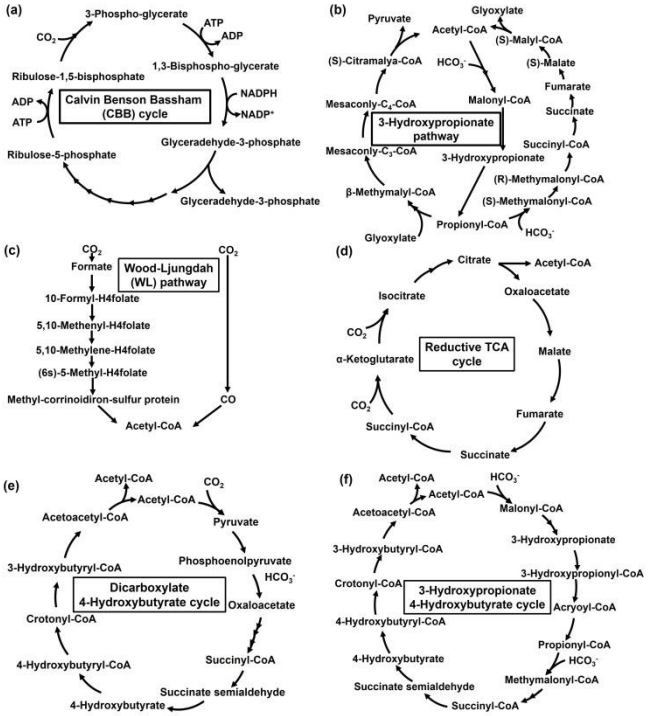

Fig. 6. Six natural CO_2 fixation pathways. (a) Calvin Benson Bassham (CBB) cycle. (b) 3-hydroxypropionate pathway. (c) Wood-Lijungdah (WL) pathway. (d)Reductive TCA cycle.(e) Dicarboxylate/4-hydroxybutyrate cycle. (f) hydroxypropionate/4-hydroxybutyrate cycle.

Visible-light driven acetate production from CO_2 with photocatalyst and microbial cells hybrid system

First, the production system for acetate, a precursor of biodegradable plastics, from CO_2 using the combination of photocatalyst and is introduced.

Visible-light driven acetate production from CO_2 using hybridisation of CdS nanoparticle and *M. thermoacetica* has been accomplished. Figure 7(A) shows the schematic representation of acetate production from CO_2 using hybridisation system of CdS nanoparticle and *M. thermoacetica* (ATCC 39073) under visible-light irradiation.[76]

In this system, acetate can be produced from CO_2 using the photosensitizing function of CdS and the WL pathway in *M. thermoacetica*. In this system, CdS is constantly regenerated by incorporating cysteine (Cys) into the reaction. Visible-light driven acetate production by *M. thermoacetica* and CdS is a two-step, one-pot synthesis as shown in Figure 7(B). First, CdS precipitation by *M. thermoacetica* is induced by adding Cd^{2+} and cysteine as sulfur sources.[77] *M. thermoacetica* performs acetate production using generated electrons from irradiated CdS nanoparticles as shown in Figure 7(B).

The Cys quenches h^+ of CdS, producing the oxidized disulfide form of cystine (CySS). The overall this process is shown in Figure 8.

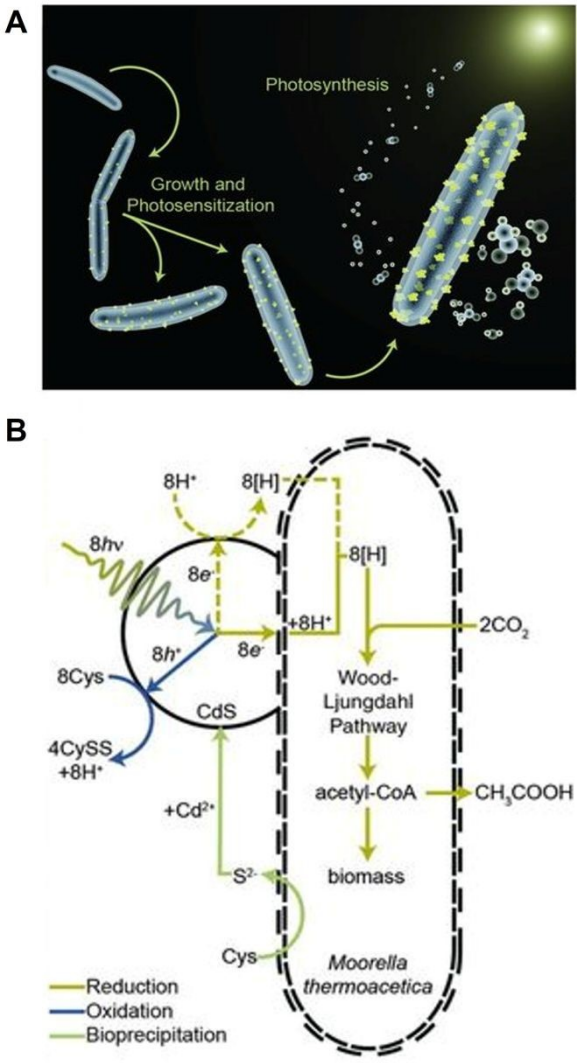

Fig. 7. Image for visible-light driven acetate production from CO_2 using hybridisation system of CdS nanoparticle and *M. thermoacetica* (A). Mechanism for visible-light driven acetate production from CO_2 using CdS nanoparticle and *M. thermoacetica* in the presence of Cys (B). Reproduced with permission from ref 76. Copyright 2016 American Association for the Advancement of Science.

$$2CO_2 + 8Cys \xrightarrow{h\nu} CH_3COOH + 2H_2O + 4CySS$$

Fig. 8. Overall process for visible-light driven acetate production form CO_2 with the hybrid system of CdS-*M. thermoacetica* in the presence of Cys.

Figure 9 shows the time dependence of acetate production with the hybrid system of CdS-*M. thermoacetica* in the presence of Cys. The irradiation source is employed an in-house fabricated circular LED array composed of 405 ± 5 nm violet LEDs with a measured photon flux of 5.5×10^{18} cm^{-2} s^{-1}. As shown in Figure 9, *ca.* 1.3 mM of acetate production is observed using the hybrid system of CdS-*M. thermoacetica* under the visible-light irradiation. On the other hand, no acetate production is observed using *M. thermoacetica* only under the visible-light irradiation. Moreover, no acetate production is observed using the hybrid system of CdS-sterilised *M. thermoacetica* under the visible-light irradiation. Also, decrease in acetate is observed under dark condition. A maximum yield of *ca*. 90% acetate based on the initial Cys concentration is accomplished using the hybrid system of CdS-*M. thermoacetica* under the visible-light irradiation. After 12 h irradiation, 1.43 mM of acetate is produced.

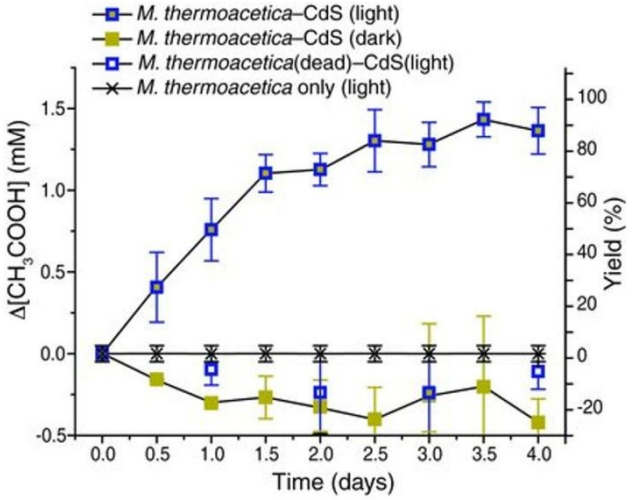

Fig. 9. Time dependence of acetate production form CO_2 with the hybrid system of CdS-*M. thermoacetica* in the presence of Cys under visible-light irradiation and dark condition. Reproduced with permission from ref 76. Copyright 2016 American Association for the Advancement of Science.

Visible light-driven acetate production using CO_2 as a raw material has also been reported using a hybrid system of gold nanoparticles (AuNPs) and *M. thermoacetica*.[78] By using this system, acetate production is estimated to be 6.01 mmol g^{-1} per week.

A tandem inorganic–biological hybrid system consisting of a TiO_2 nanoparticle loaded with a manganese(II) phthalocyanine (MnPc) cocatalyst, CdS and *M. thermoacetica* capable of oxygenic photosynthesis of acetate from CO_2 has been reported.[79] Figure 10(A) shows the schematic representation of acetate production from CO_2 using hybridisation system of CdS nanoparticle and *M. thermoacetica* under visible-light irradiation.

A feature of this system is that the photooxidation catalyst TiO_2 is loaded with the cocatalyst MnPc to regenerate the CySS/Cys redox shuttle, coupling the water oxidation and CySS reduction. Figure 10(B) shows the time dependence of acetate production with the tandem system of TiO_2 nanoparticle loaded with MnPc, CdS and *M. thermoacetica* in the presence of Cys. The irradiation source is employed a filtered 75 W Xenon lamp (AM1.5G, 5% Sun).

As shown in Figure 11, comparing CdS-*M. thermoacetica* and MnPc-loaded TiO_2 to the control, the combined tandem system shows increased acetate production. Both CdS-*M. thermoacetica* alone and the MnPc-loaded TiO_2-*M. thermoacetica* control shows reduced acetate production below the stoichiometric limit imposed by Cys. Without MnPc, the TiO_2-only tandem system performed poorly. Comparison of the cumulative electron equivalents of acetate ($8e^-$) and O_2 ($4e^-$) measured over a 3.5-day period shows a strong correlation between the reduced product, acetate and the oxidized product, O_2. By using this system, 1.2 mM of acetate is produced after 1 day.

View Article Online
DOI: 10.1039/D0CC00217B

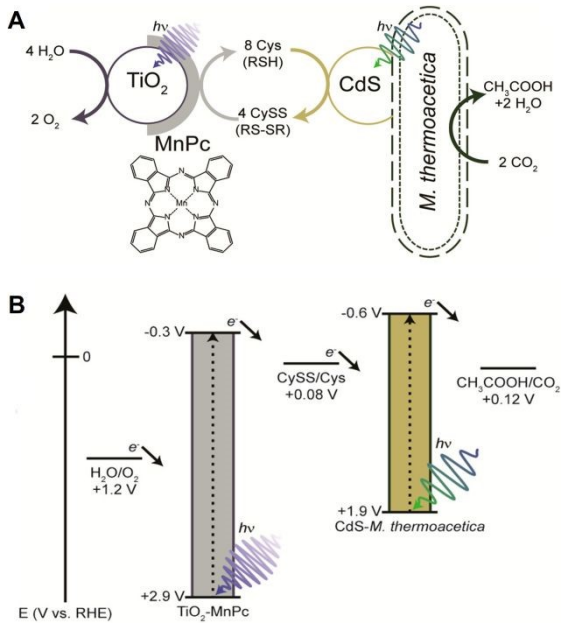

Fig. 10. Visible-light driven acetate production from CO_2 using hybridisation system of TiO_2 nanoparticle loaded with MnPc, CdS nanoparticle and *M. thermoacetica* (A). Energy level diagram depicting the relative alignment of the TiO_2 and CdS with the relevant redox processes (B). Reproduced with permission from ref 79. Copyright 2016 American Chemical Society.

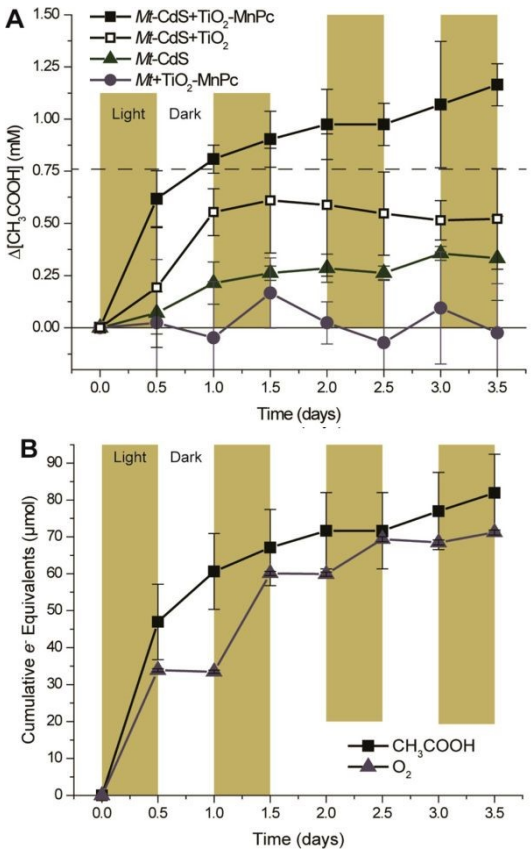

Fig. 11. Time dependence of acetate production form CO_2 with the tandem system of TiO_2 nanoparticle loaded with MnPc, CdS and *M. thermoacetica* in the presence of Cys under visible-light irradiation (■) (A). □: Tandem system of TiO_2 nanoparticle, CdS and *M. thermoacetica*, ▲: hybrid system of CdS and *M. thermoacetica*, ●: hybrid system of TiO_2 nanoparticle loaded with MnPc and *M. thermoacetica*. Time dependence of the amount of acetate and oxygen produced with the tandem system of TiO_2 nanoparticle loaded with MnPc, CdS and *M. thermoacetica* in the presence of Cys under visible-light irradiation (B). Reproduced with permission from ref 79. Copyright 2016 American Chemical Society.

A visible-light-driven acetate production from CO_2 has been reported in which perylene diimide derivatives (PDI) and poly(fluorene-*co*-phenylene) (PFP) are applied to the *M. thermoacetica* surface as photosensitizers to form a p-n heterojunction (PFP/PDI) layer as shown in Figure 12(A).[80]

The accumulated acetate yield of PDI/PFP/*M. thermoacetica* (*ca*. 0.63 mM) is significantly higher than that of PDI/*M. thermoacetica* (*ca.* 0.25 mM) or PFP/*M. thermoacetica* (*ca*. 0.4 mM) under the irradiation with a Xenon fiber optic lamp with filters larger than 420 nm. Figure 12(B) shows the time dependence of produced acetate using PDI/PFP/*M. thermoacetica* in an alternating light-dark cycle of 12 h each.

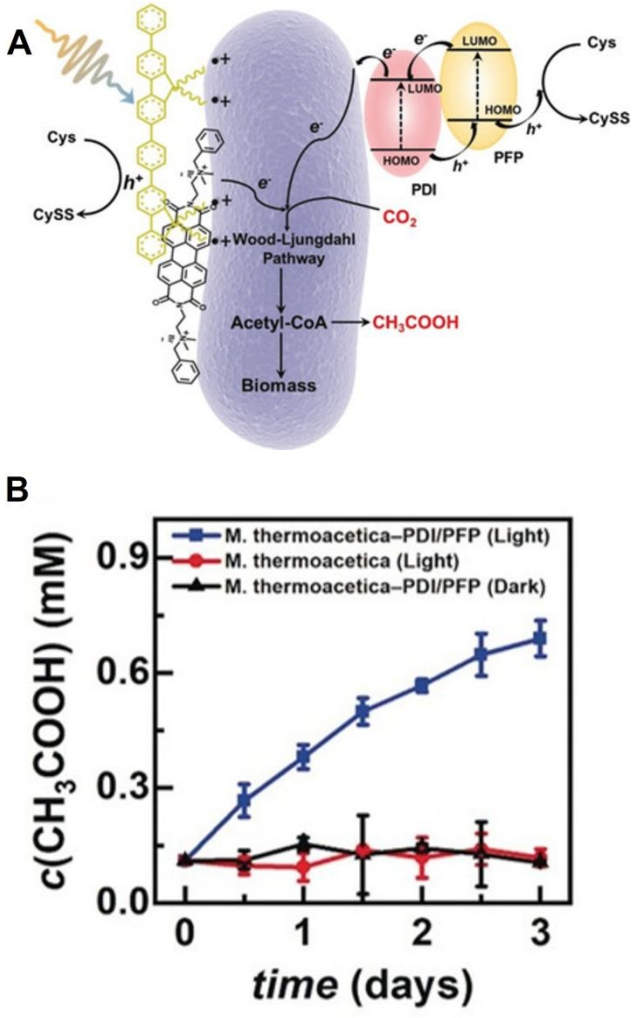

Fig. 12. Visible-light driven acetate production from CO_2 using PDI/PFP/*M. thermoacetica* hybrid system (A). Time dependence of acetate production form CO_2 with PDI/PFP/*M. thermoacetica* hybrid system in the presence of Cys under visible-light irradiation (■) . ■: Only *M. thermoacetica*, ▲: dark condition (B). Reproduced with permission from ref 80. Copyright 2020 Wiley-VCH Verlag GmbH & Co. KGaA, Weinheim.

After 3 days incubation with irradiation, the accumulation amount of the acetate is estimated to be 0.63 mM. The quantum yield of 1.6 % is calculated based on the initial Cys concentration. Here, the quantum yield is calculated from the following equation (1) (*n*: number of electrons, C: total acetate concentration, V: total suspension volume, ϕ (cm^{-2} s^{-1}): photo flux, A: area of illumination, t: reaction time, N_A: Avogadro's

View Article Online
DOI: 10.1039/D6CC00717F

Number). Acetate is produced by the 8-electron reduction of CO_2, therefore the *n* value is 8.

$$\text{Quantum yield}(\%) = \frac{n\,\mathrm{C}\,\mathrm{V}\,\mathrm{N_A}}{\Phi\,\mathrm{t}\,\mathrm{A}} \times 100 \qquad (1)$$

(*n*: number of electrons, C: total acetate concentration, V: total suspension volume, ϕ (cm^{-2} s^{-1}): photo flux, A: area of illumination (5 cm^2), t: reaction time, N_A: Avogadro's Number).

Sporomus ovata (*S. ovata*) is a type of bacteria characterized by banana-shaped cells. *S. ovata* cells are strictly anaerobic, Gram-negative, spore-forming, straight or slightly curved rods that are motile by lateral flagella.[81] There has been much research into the electrosynthesis of energy-containing carbon chains using *S. ovata*.[82,83] *S. ovata* is a candidate biological catalyst that converts sunlight, water, and CO_2 into oxygen and liquid fuel or variable chemicals.

Visible-light driven acetate production from CO_2 using hybridisation of CdS nanoparticles and *S. ovata* (CdS-*S. ovata*) also has been accomplished. Figure 13 (A) shows the schematic representation of acetate production from CO_2 using CdS-*S. ovata* under visible-light irradiation.[84]

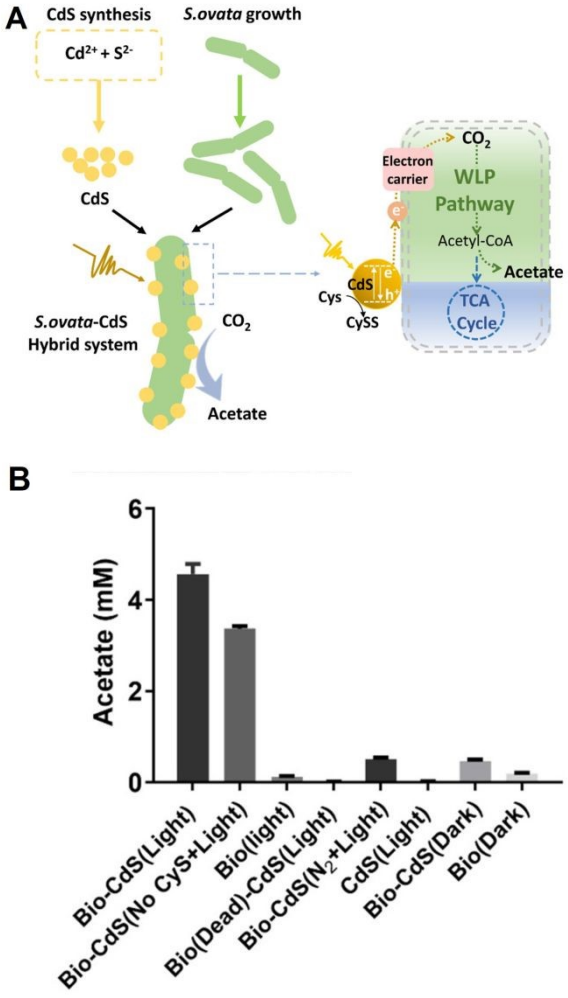

Fig. 13. Schematic representation of visible-light driven acetate production from CO_2 using CdS-*S. ovata* (A). Acetate production using CdS-*S. ovata* after 1 day of light irradiation in the presence of Cys. Bio-CdS (No CyS + Light): in the absence of Cys, Bio (light): only *S. ovata*, Bio(Dead)-CdS (Light): sterilized *S. ovata* and CdS hybrid system, Bio-CdS (N_2 + Light): without CO_2 gas, CdS (Light): only CdS. Dark: under dark conditions (B). Reproduced with permission from ref 84. Copyright 2020 American Chemical Society.

In this system, photoelectrons are generated by CdS under light irradiation and transferred to *S. ovata* to achieve acetate production using CO_2 as a raw material via the WL pathway. In this system, it is found that formate is produced as an intermediate, and then rapidly is converted to the final product, acetate. Figure 13(B) shows the visible-light driven acetate production using CdS-*S. ovata* after 1 day of light irradiation and the controls in the presence of Cys. The intensity of light (400 ± 5 nm) is estimated to be 0.20 mW cm^{-2}. Each experiment is pressurized with 2.0 atm 80% N_2 and 20% CO_2. In this figure, Bio-CdS means CdS-*S. ovata*. As shown in Figure 13(B), a high concentration of acetate is observed using CdS-*S. ovata* during the visible-light irradiation in contrast to the other systems. By using CdS-*S. ovata*, the quantum yield reaches to 16.8 ± 9%, and the active duration time of the system can last for 5 days. The quantum yield also is estimated using equation (1).

Visible light-driven acetate production from CO_2 by the hybridization of a Z-scheme semiconductor photocatalytic system with *S. ovata* has been reported as shown in Figure 14(A).[85] In this system, Z-scheme consists of particulate semiconductors La and Rh co-doped $SrTiO_3$ ($SrTiO_3$: La, Rh) and Mo-doped $BiVO_4$ ($BiVO_4$: Mo). In this system, photocatalytic particles are immobilised onto a sheet.

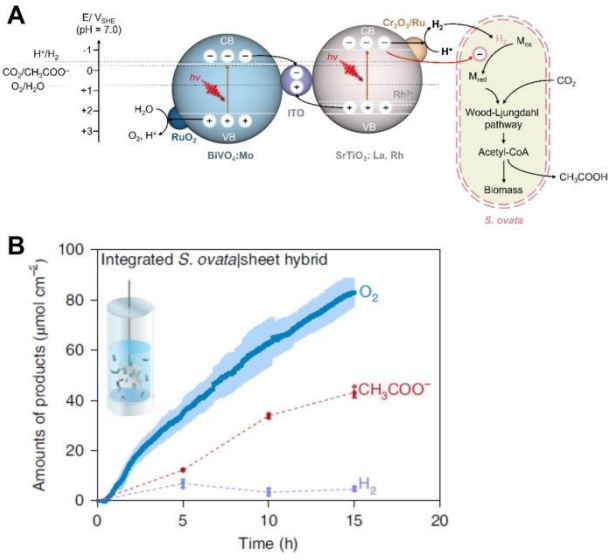

Fig. 14. Schematic representation of visible light-driven acetate production from CO_2 by the hybridization of a Z-scheme semiconductor photocatalytic system consisting of $SrTiO_3$: La, Rh and $BiVO_4$: Mo with *S. ovata* (A). Time course of photosynthetic acetate, O_2 and H_2 production over *S. ovata*|Cr_2O_3/Ru-$SrTiO_3$:La,Rh|ITO|RuO_2-$BiVO_4$:Mo hybrids(B). Reproduced with permission from ref 85. Copyright 2022, The Authors, under exclusive licence to Springer Nature Limited

By using hybridization of a Z-scheme semiconductor photocatalytic system consisting of $SrTiO_3$: La, Rh and $BiVO_4$: Mo with *S. ovata*, *ca.* 40 and 80 μmol cm^{-2} of acetate and oxygen production are observed after 15 h with 1 sun (AM 1.5G, 100 mW cm^{-2}) irradiation as shown in Figure 14(B). The mixture gases of 80% N_2 and 20% CO_2 are used for this system. The solar energy to acetate efficiency is estimated to be 0.70 ± 0.04% and the apparent quantum yield is calculated to be 21.3% at 420 ± 15 nm. The quantum yield also is estimated using equation (1) in this experiment.

Visible light-driven acetate production from CO_2 by system hybridising semiconducting polymer with *S. ovata* are also being studied.[86] The polymer semiconductor poly(3-hexylthiophene) (P3HT; chemical structure is shown in Figure 15), widely used in the organic photovoltaic field,[87,88] is applied in this system.

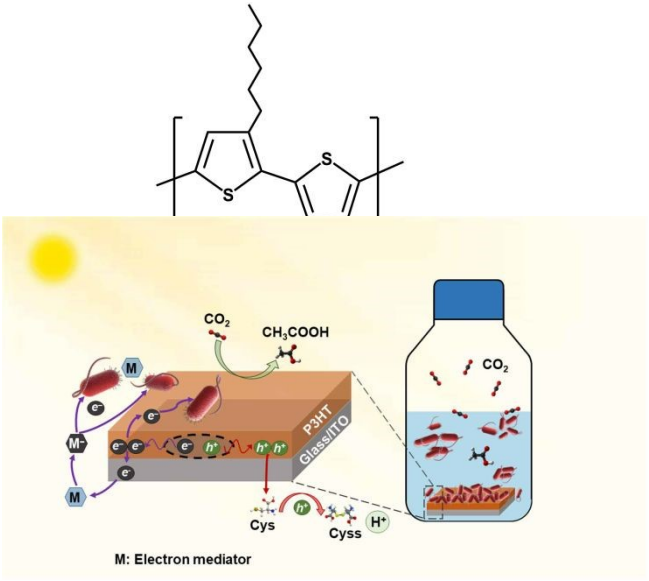

Fig. 15. Chemical Structure of P3HT.

Figure 16 shows the schematic representation of visible-light driven acetate production from CO_2 using the system of P3HT immobilised onto indium tin oxide coated glass substrate (ITO) and *S. ovata* in the presence of Cys and an electron mediator (M).

Fig. 16. Schematic representation of visible light-driven acetate production from CO_2 by the system of PSHT immobilised ITO substrate with *S. ovata* in the presence of Cys and M. Reproduced with permission from ref 86. Copyright 2024 American Association for the Advancement of Science.

Figure 17 shows a schematic diagram of the exciton generation, separation, and transport processes in a P3HT, [6,6]-phenyl-C_{61}-butyric acid methyl ester (P3HT: PCBM) heterojunction (bulk heterojunction (BHJ)), and a film with an ITO/ZnO/P3HT:PCBM/MoO_3 multilayer structure.

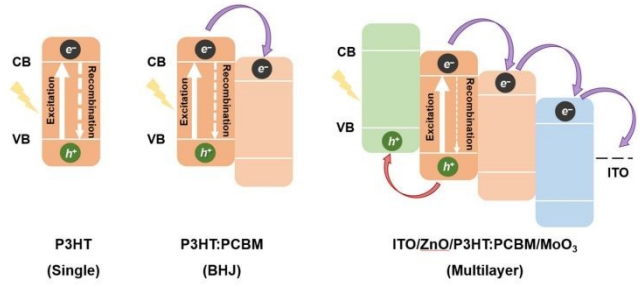

Fig. 17. Schematic diagrams for exciton separation and recombination of polymer semiconductor films with P3HT, P3HT: PCBM bulk-heterojunction (BHJ), and multilayer film structures. CB, conduction band; VB, valence band. Reproduced with permission from ref 86. Copyright 2024 American Association for the Advancement of Science.

Here, visible light-driven acetate production from CO_2 is investigated using a hybrid system of each P3HT-immobilised device and *S. ovata*. Cys and potassium ferricyanide are added as hole-trapping agents and electron mediators, respectively. The LED white light is used as an irradiation source with adjustable light intensity. The mixture gases of 80% N_2 and 20% CO_2 are used as carbon sources for this system. Figure 18 shows total amount of acetate production from CO_2 using a hybrid system of each P3HT-immobilised device and *S. ovata*.

Fig. 18. Total acetate production with a hybrid system of P3HT-immobilised device and *S. ovata* after 1 week of light irradiation in the presence of Cys and potassium ferricyanide. Reproduced with permission from ref 86. Copyright 2024 American Association for the Advancement of Science.

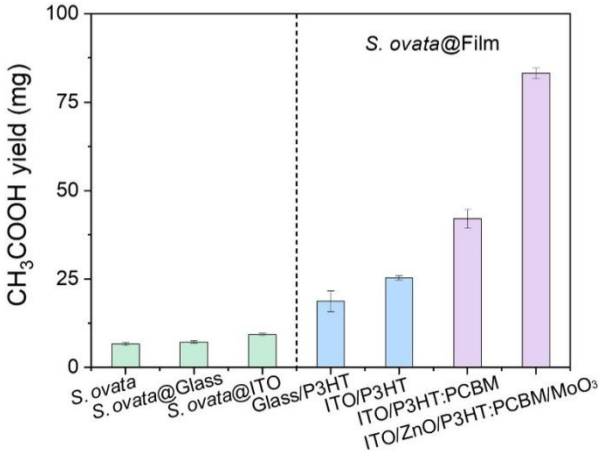

It is found that the acetate production is improved by using the hybrid system of ITO/ZnO/P3HT:PCBM/MoO_3 multilayer and *S. ovata* compared to other devices as shown in Figure 18. The quantum yield of the hybrid system of ITO/ZnO/P3HT:PCBM/MoO_3 multilayer and *S. ovata* reaches about 10%, which is obviously higher than 0.5% of the control system without polymer semiconductor device. Also in this experiment, the quantum yield is estimated using equation (1).

Visible light-driven acetate production from CO_2 by system hybridising InP/ZnSe/ZnS quantum dots (QDs) with *S. ovata* in the presence of Cys and potassium ferricyanide is studied.[89] InP with a bandgap of 1.35 eV and a Bohr radius of approximately 10 nm can effectively absorb visible light.[90] Figure 19(A) shows the schematic representation of visible-light driven acetate production from CO_2 using the hybridising system of InP/ZnSe/ZnS QDs and *S. ovata*.

By growing a multilayer shell of ZnSe and ZnS on InP QDs synthesized by the hot injection method, the surface of the QDs can be passivated and the stability of the InP QDs can be improved.[91,92] Furthermore, the low biotoxicity of InP QDs makes it potentially promising biological hybrid materials.[93]

In this system Cys and potassium ferricyanide also are added as hole-trapping agents and electron mediators, respectively. The Xenon lamp with an AM 1.5 G filter is used as the irradiation source with light intensity adjusted. The mixture gases of 80% N_2 and 20% CO_2 are used as carbon sources for this system. Figure 20(B) shows total amount of acetate production from CO_2 using the hybridising system of InP/ZnSe/ZnS QDs and *S. ovata*. It is found that the acetate production is improved by using the hybridising system of InP/ZnSe/ZnS QDs and *S. ovata* in the presence of ferricyanide compared to other conditions as shown in Figure 20(B). The quantum yield of the hybridising system of InP/ZnSe/ZnS QDs and *S. ovata* in the presence of ferricyanide reaches about 7.0% estimated using equation (1).

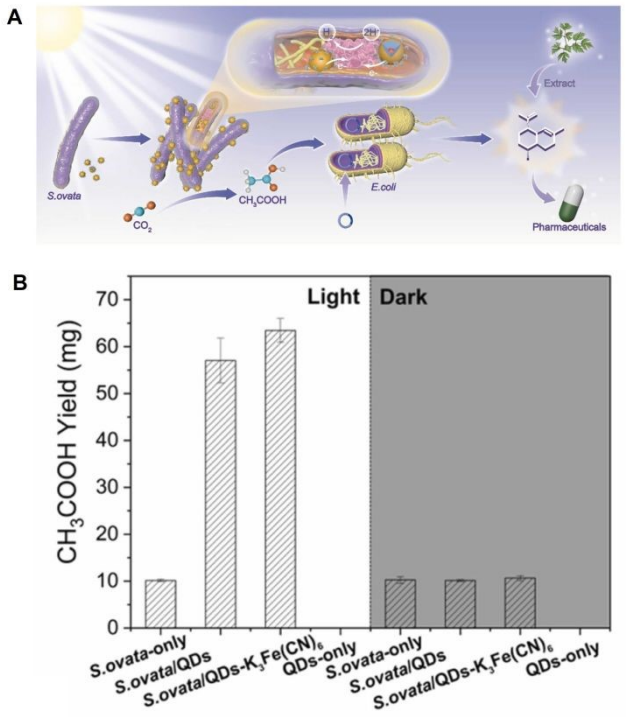

Fig. 19. Schematic representation of visible light-driven acetate production from CO_2 by the hybridising system of InP/ZnSe/ZnS QDs and *S. ovata* (A). Total acetate production with the hybridising system of InP/ZnSe/ZnS QDs and *S. ovata* after 1 week of light irradiation in the presence of Cys and potassium ferricyanide (B). Reproduced with permission from ref 89. Copyright 2022 Elsevier Ltd.

Visible-light driven acetate production from CO_2 using photoelectrochemical cell consisting of silicon nanowire integrated *S. ovata* as a photocathode has been reported as shown in Figure 20.[94]

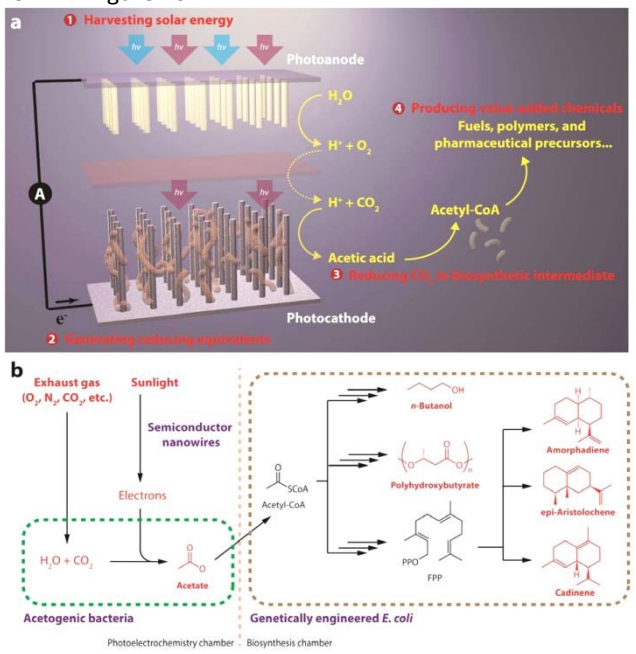

Fig. 20. Schematic representation of photoelectrochemical cell consisting of silicon nanowire integrated *S. ovata* (a) The proposed approach for solar-powered CO_2 fixation includes four general components: (1) harvesting solar energy, (2) generating reducing equivalents, (3) reducing CO_2 to biosynthetic intermediates, and (4) producing value-added chemicals. An integration of materials science and biology, such an approach combines the advantages of solid-state devices with living organisms. (b) As a proof of concept, under mild conditions sunlight can provide the energy to directly treat exhaust gas and generate acetate as the biosynthetic intermediate, which is upgraded into liquid fuels, biopolymers, and pharmaceutical precursors and so on. FPP: farnesyl pyrophosphate. Reproduced with permission from ref 94. Copyright 2015 American Chemical Society.

By using photoelectrochemical cell consisting of silicon nanowire integrated *S. ovata*, visible-light acetate production is accomplished. Moreover, variable organic molecules also are produced by using hybridisation system of engineered *E. coli* with this photoelectrochemical cell. In addition, it has also been found that acetate production is improved by using methanol-adapted *S. ovata* in this system.[95]

Visible-light driven production of the other plastic precursor from CO_2 with photocatalyst and microbial cells hybrid system

The other plastic precursors that can be produced from CO_2 driven by visible light using a photocatalyst and microbial cells hybrid system are introduced.

Shikimic acid is a precursor for lignin production and can be a raw material for bioplastics.[96]

Visible-light driven shikimic acid production with the system of polyphenol-functionalised indium phosphide (InP) with common heterotrophs, *Saccharomyces cerevisiae* (*S. cerevisiae*) has been reported as shown in Figure 21.[97] In this system, yeast strain *S. cerevisiae* Δ*zwf1* is selected. *S. cerevisiae* Δzwf1 is genetically engineered to overexpress four genes to enhance carbon flux through the shikimic acid pathway.[98]

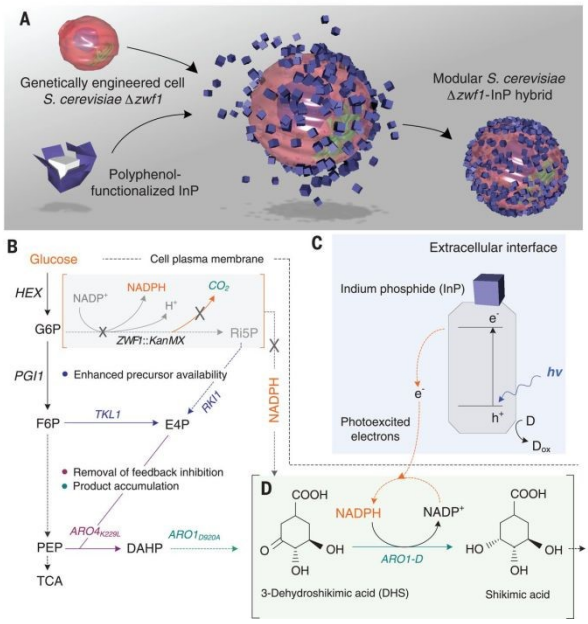

Fig. 21. Schematic diagrams for preparation of InP-*S. cerevisiae* Δzwf1 (A). Metabolic engineering diagram for overproduction of shikimic acid. *S. cerevisiae* Δ*zwf1* has the oxidative pentose phosphate pathway disrupted (*ZWF1*), leading to low cytosolic NADPH pools, which directly affects the shikimic acid pathway and reduces carbon loss in the production of CO_2 (B). Schematic of cellular NADPH regeneration and shikimic acid biosynthesis assisted by photogenerated electrons from InP nanoparticles (C and D). G6P, glucose-6-phosphate; F6P, fructose-6-phosphate; Ri5P, ribulose-5-phosphate; E4P, erythrose-4-phosphate; PEP, phosphoenolpyruvate; DAHP, 3-deoxy-d-arabinoheptulosonate-7-phosphate; HEX, hexokinase; ZWF1, glucose-6-phosphate 1-dehydrogenase; PGI1, phosphoglucose isomerase; RKI1, ribose-5-phosphate ketol-isomerase; TKL1, transketolase; $ARO4_{K229L}$, feedback-insensitive DAHP synthase; $ARO1_{D920A}$, mutant pentafunctional aromatic enzyme; TCA, tricarboxylic acid cycle; h, Planck's constant; ν, frequency; h^+, electron hole; e^-, electron; D, putative electron donors in the cell culture medium; D_{ox}, oxidized electron donor species. Reproduced with permission from ref 97. Copyright 2018 American Association for the Advancement of Science.

Figure 22 shows the specific shikimic acid production with the system using InP-*S. cerevisiae* Δzwf1 under visible-light irradiation (5.6 mW cm^{-2}). The specific shikimic acid production with *S. cerevisiae* Δzwf1 or wild-type *S. cerevisiae* under the condition of dark incubation also is shown in Figure 22. As shown in Figure 22, the specific shikimic

acid production increases using InP-*S. cerevisiae* Δzwf1 under visible-light irradiation compared with that of the system using *S. cerevisiae* Δzwf1 or wild-type *S. cerevisiae* under the dark conditions.

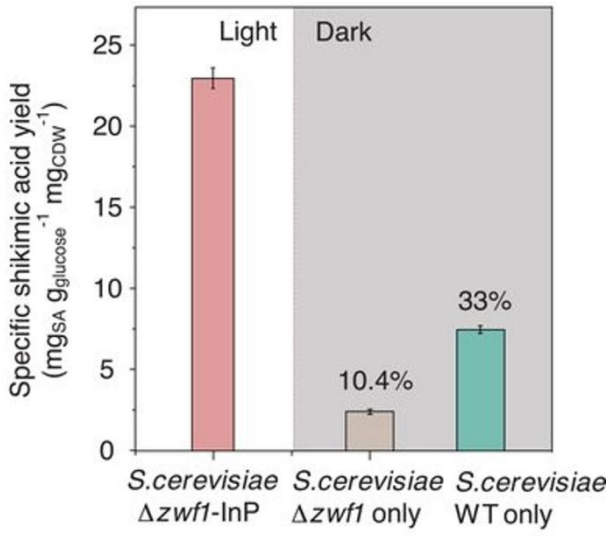

Fig. 22. Total shikimic acid production with InP-*S. cerevisiae* Δzwf1 under visible-light irradiation (5.6 mW cm^{-2}), with *S. cerevisiae* Δzwf1 or wild-type *S. cerevisiae* under the condition of dark incubation. Reproduced with permission from ref 97. Copyright 2018 American Association for the Advancement of Science.

3-Hydroxybutanone (acetoin) and 2,3-butanediol are two important four-carbon platform compounds with pharmaceutical and chemical synthesis applications.[99-102] (*S,S*)-Butane-2,3-diol is produced from acetoin in the presence of NADH with (S,S)-butanediol dehydrogenase (BDH; EC EC 1.1.1.76) as shown in Figure 23.[103-105]

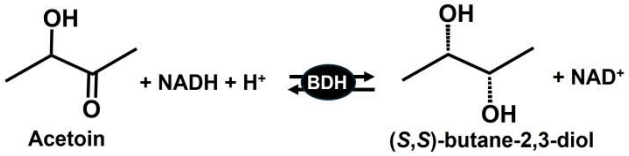

Fig. 23. BDH-catalysed (*S,S*)-butane-2,3-diol production from acetoin in the presence of NADH

Visible-light driven acetoin production from CO_2 with the hybrid system of eosin Y and *Ralstonia eutropha* (*R. eutropha*) has been reported.[106] *R. eutropha* has attracted significant research attention due to its excellent CO_2 fixation capacity and potential for expanding production diversity.[107] Figure 24 shows the schematic representation of the hybrid system of eosin Y and *R. eutropha* for visible-light acetoin production from CO_2. In this system, eosin Y specifically binds to the membrane-bound hydrogenase (MBH) of *R. eutropha* and achieves targeted electron transfer to the hydrogenase-mediated electron transport and transformation pathway of *R. eutropha* (pathway I). To enhance ATP synthesis, an oxygen-independent proton pump (*Gloeobacter rhodopsin*) is introduced into *R. eutropha* (pathway II). To promote carbon metabolic flux towards acetoin production, the by-product biosynthetic pathway is blocked (pathway III). The genetically engineered *R. eutropha* strain named REH01 is used in this system.

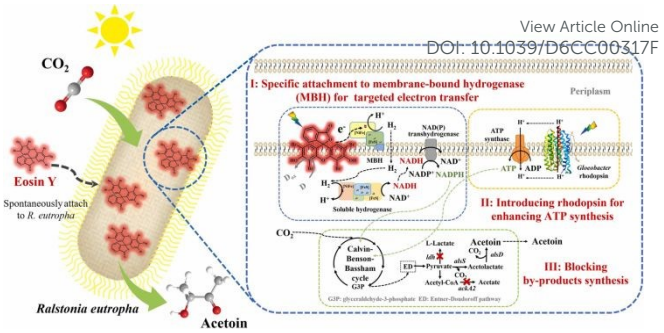

Fig. 24. Visible-light driven acetoin production from CO_2 with the hybrid system of eosin Y and *R. eutropha*. Reproduced with permission from ref 106. Copyright 2025 The Authors. Published by Elsevier Ltd. Creative Commons CC-BY license.

Figure 25(A) shows the time dependence of acetoin production with the hybrid system of eosin Y and REH01 during visible-light irradiation using LED lamps (λ=520 nm) with a certain light intensity (2, 5, or 10 mW cm^{-2}). Throughout the reaction, a mixture gas of CO_2/O_2 (molar ratio: 99/1) is continuously sparged into the reaction system. In this figure, Biohybrid means the hybrid system of eosin Y and REH01.

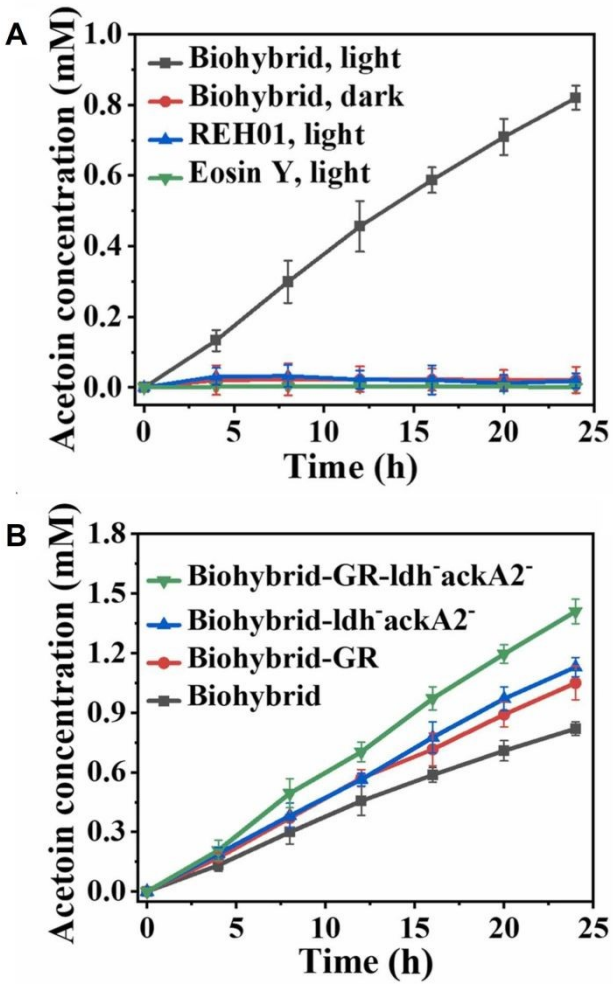

Fig. 25. Time dependence of acetoin production from CO_2 using the hybrid system of eosin Y and REH01 during visible-light irradiation. Red: dark condition, Blue: only REH01, Green: only eosin Y (A). Time dependence of acetoin production from CO_2 using the hybrid system of eosin Y and REH01 during visible-light irradiation. Green: eosin Y and GR expressing REH01 without *ldh* and *ackA2*. Bule: eosin Y and REH01 without *ldh* and *ackA2*. Red: eosin Y and GR expressing REH01. Black: eosin Y and REH01 (B). Reproduced with permission from ref 106. Copyright 2025 The Authors. Published by Elsevier Ltd. Creative Commons CC-BY license.

View Article Online
DOI: 10.1039/D6CC00317F

As shown in Figure 25(A), *ca.* 0.8 mM of acetoin production is observed after 24 h irradiation. On the other hand, little acetoin production has been observed under other conditions. Furthermore, metabolic engineering strategies have been employed to enhance the acetoin-producing capability of REH01. REH01 strains lacking the GR and/or *ldh* and *ackA2* genes have been prepared. Figure 25(B) shows the time dependence of acetoin production with the hybrid system of eosin Y and genetically modified REH01 during visible-light irradiation. As shown in Figure 25(B), the engineered eosin Y-GR expressing REH01 without *ldh* and *ackA2.* biohybrid system achieves an acetoin yield of 1.41 ± 0.06 mM, representing 2.07 times larger than that of H_2-supplied autotrophic fermentation. Therefore, carbon flux can be directed towards acetoin production by inhibiting the L-lactate and acetate biosynthetic pathways.

Visible-light driven polyhydroxybutyrate (PHB) production from CO_2 with photocatalyst and microbial cells hybrid system

Among biodegradable plastics based on aliphatic polyesters, plastics derived from poly-3-hydroxybutyrate (PHB) are attractive because are compostable, made from renewable feedstocks, and biodegradable.[108-115] The PHB can be produced from CO_2 driven by visible light using a photocatalyst and microbial cells hybrid system are introduced. Hydrogen-oxidizing bacterium, *Raistonia eutropha* has been used as a microbial cell for PHB production.[116]

The PHB production using electrochemical system of cobalt-phosphorus (Co-P) alloy cathode and cobalt phosphate (CoP_i) anode with *Ralstonia eutropha* has been reported for the first time.[117]

Visible-light driven PHB production with the system of photocatalyst graphitic carbon nitride (g-C_3N_4) and *Ralstonia eutropha* H16 in the presence of triethanol amine (TEOA) has been reported as shown in Figure 26(A).[118] As shown in Figure 26(A), PHB is produced in *Ralstonia eutropha* H16 by utilizing the TCA cycle, Calvin-Benson-Bassham (CBB) cycle, NADH regeneration, and hydrogen.

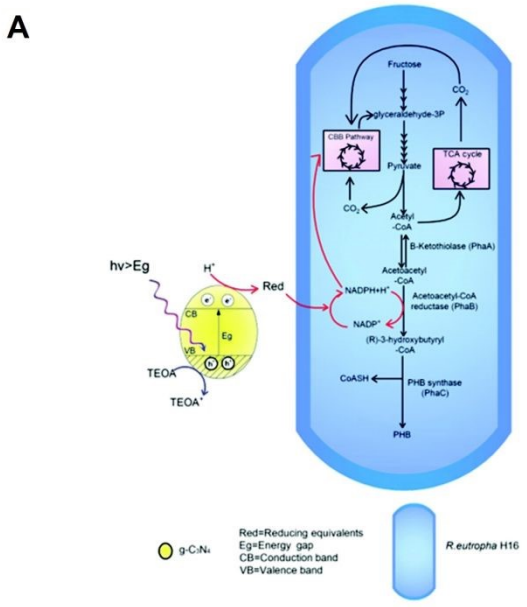

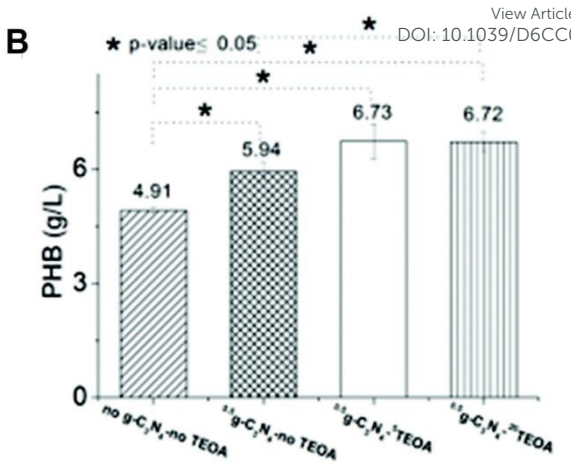

Fig. 26. Schematic representation for the visible-light driven PHB production from CO_2 or fructose with the system of g-C_3N_4 and *Ralstonia eutropha* H16 in the presence of TEOA (A). Total PHB production with the system of g-C_3N_4 and *Ralstonia eutropha* H16 in the presence of TEOA after 96 h irradiation with the LED light set at 4200 lux (B). Reproduced with permission from ref 118. Copyright 2019 The Royal Society of Chemistry.

Figure 26(B) shows the total amount of PHB production using g-C_3N_4 and *Ralstonia eutropha* H16 in the presence of TEOA after 96 h irradiation with the LED light set at 4200 lux. This figure also shows the amount of PHB produced in the absence of TEOA or g-C_3N_4. After 96 h irradiation, PHB production is improved 1.4 times to 6.73 ± 0.45 g l^{-1} with the system using g-C_3N_4 and *Ralstonia eutropha* H16 in the presence of TEOA. On the other hand, decreasing PHB production is observed using only *Ralstonia eutropha* H16 or without g-C_3N_4.

The development of a water-splitting enzymatic photocatalyst made of g-C_3N_4 coupled with H_2O_2-degrading catalase and its utilisation for hybrid system with *Ralstonia eutropha* for the visible-light driven PHB production as shown in Figure 27(A).[119] By using catalase, it is possible to decompose hydrogen peroxide produced due to the two-electron oxidation of water into oxygen[120] by g-C_3N_4.[121.]

Figure 27(B) shows the total amount of PHB production using catalase modified g-C_3N_4 and *Ralstonia eutropha* H16 after 48 h irradiation with 500 W Xe lamp with an AM1.5G filter. This figure also shows the amount of PHB produced using the system only *Ralstonia eutropha* H16, without g-C_3N_4, without catalase and dark condition.

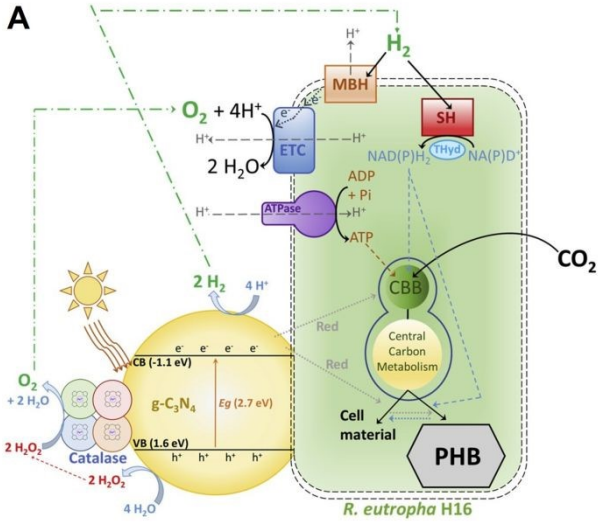

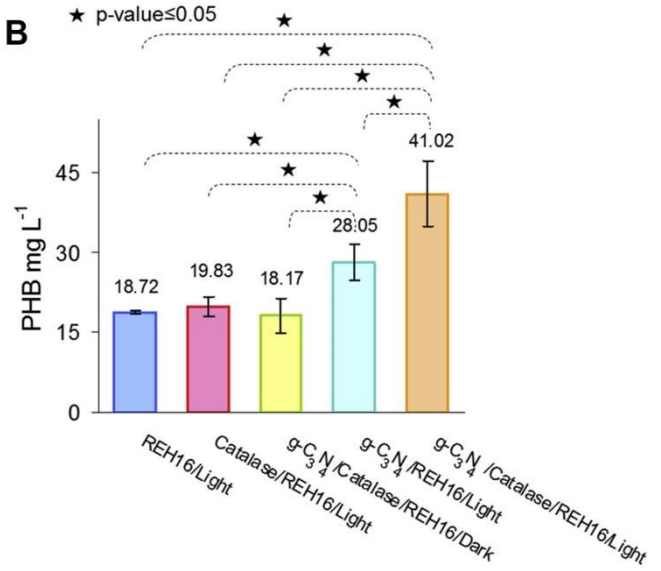

Fig. 27. Schematic representation for the visible-light driven PHB production from CO_2 with the system of catalase modified g-C_3N_4 and *Ralstonia eutropha* H16 (A). Total PHB production with the system of catalase modified g-C_3N_4 and *Ralstonia eutropha* H16 after 48 h irradiation with 500 W Xe lamp with an AM1.5G filter (B). Reproduced with permission from ref 119. Copyright 2020 The authors Creative Commons CC-BY-NC-ND license.

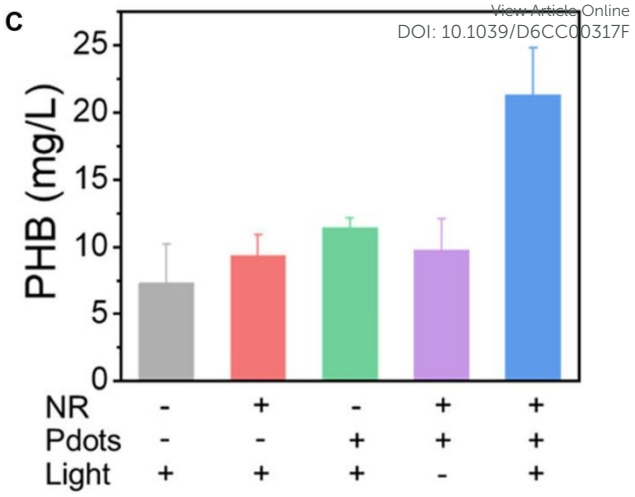

Fig. 28. Schematic representation of visible-light driven PHB production from CO_2 with *RH16*/NR/Pdots (A) Metabolic pathway of PHB production from CO_2 in *RH16*. 3HB-CoA: 3-hydroxybutyryl-CoA; PHB: polyhydroxybutyrate; h^+: electron hole; e^-: electron; Cys: cysteine; CySS: cystine; NR_{ox}: the oxidized state of NR; NR_{red}: the reduced state of NR. (B) Schematic diagram for Pdots promoting the PHB production with *RH16*. Total PHB production with the system of *RH16*/NR/Pdots in the presence of Cys after 48 h irradiation. "-" and "+" mean non-additive and added, respectively(C). Reproduced with permission from ref 123. Copyright 2022 American Chemical Society.

The hybrid system built with the water-splitting g-C_3N_4-catalase photocatalyst doubles the production of the PHB by *Ralstonia eutropha* H16 from CO_2 and increases it by 1.84-fold from fructose. After 48 h irradiation, *ca.*41 mg of PHB production is observed by using catalase modified g-C_3N_4 and *Ralstonia eutropha* H16 without any sacrificial electron donor reagent such as TEOA.

Visible-light driven PHB production from CO_2 with the system of conjugated polymer dots (Pdots) consisting of Poly[N-9′-heptadecanyl-2,7-carbazole-alt-5,5-(4′,7′-di-2-thienyl-2′,1′,3′-benzo-thiadiazole) (PFODTBT) and triblock copolymer ABA, poly(*N*, *N*-dimethylamino ethyl methacrylate)-*B*-poly(9,9-*N*-dihyxyl-2,7-fluorene)-*B*-poly(*N*, *N*-dimethylamino ethyl methacrylate) and PS-PEG-COOH (copolymer polystyrene grafted with carboxy-terminated polyethylene oxide) (PFODTBT Pdots)[122] and *Ralstonia eutropha* H16 (*RH16*/NR/Pdots) has been reported as shown in Figures 28(A) and (B).[123] In this system, Cys and neutral red (NR) are used as an electron donor and an electron mediator as the example of Figure 5(b). A Xenon fiber optic lamp with filters is employed with an AM 1.5G filte. The optimal optical power density is determined to be 2.5 mW cm^{-2}. The mixture gases of 80% N_2 and 20% CO_2 are used as carbon sources for this system. Under light irradiation, the PHB production of *RH16* is estimated to be only 7.3 ± 2.91 mg L^{-1} due to accumulation in the initial stage of autotrophic as shown in Figure 28(C).

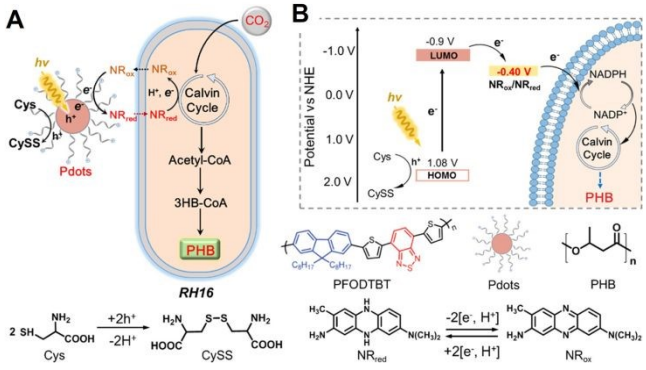

The PHB production s of *RH16*/Pdots, *RH16*/NR, and *RH16*/NR/Pdots (under dark conditions) are estimated to be 9.3 ± 1.56, 11.4 ± 0.76, and 9.8 ± 2.35 mg L^{-1}, respectively.

As shown in Figure 28(C), the production of PHB from the biohybrid system is slightly higher than that of RH16, suggesting that the addition of Pdots and NR is responsible for the increased amount of PHB in solution. Under visible-light irradiation, the cumulative PHB production of *RH16*/NR/Pdots (21.3 ± 3.78 mg L^{-1}) increases significantly, which is an increase of 192% compared with only *RH16*. It is mainly because the visible-light induced generated electrons of Pdots could be effectively transferred to the inside of *RH16* by NR.

Visible-light driven PHB production with the system of photocatalyst g-C_3N_4 and *Rhodopseudomonas palustris* (*R. palustris*)[124] in the presence of sulfur nanoparticles (SNPs) (g-C_3N_4–SNPs–*R. palustris*) has been reported as shown in Figure 29 (A).[125] In this system, SNPs act as dual electron donor as shown in Figure 29(A).

Figure 29(B) shows the total PHB production with the system of g-C_3N_4–SNPs–*R. palustris* under irradiation with the simulated daylight (~7000 lux) after 8 days. The mixture gases of 80% N_2 and 20% CO_2 are used as carbon sources for this system. Figure 29(B) shows the PHB concentrations and percentage of cell dry weight occupied by PHB on day 8 (grey line).

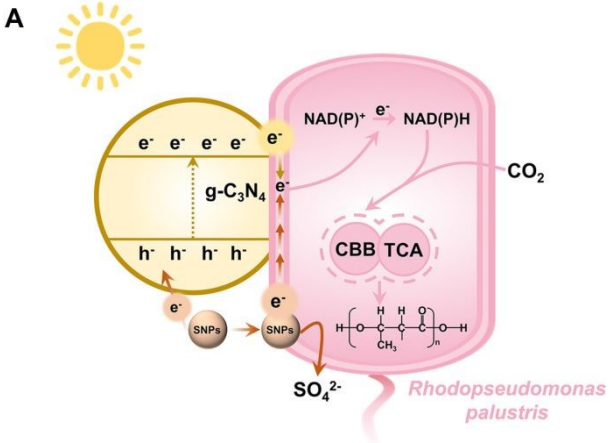

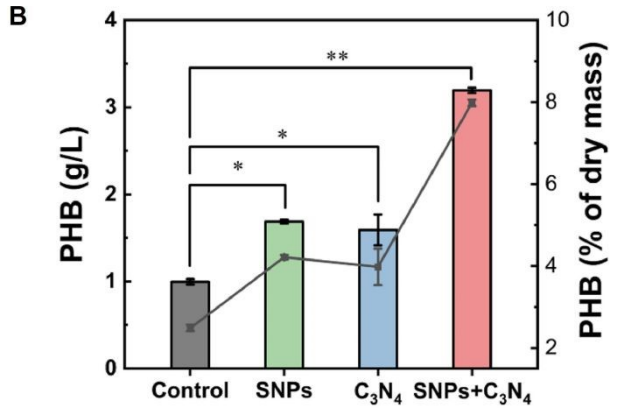

Fig. 29. Schematic representation for the visible-light driven PHB production from CO_2 with the system of g-C_3N_4–SNPs–*R. palustris* (A). Total PHB production from CO_2 with the system of g-C_3N_4–SNPs–*R. palustris* after 8 days irradiation(B). Reproduced with permission from ref 125. Copyright 2025 The Research Center for Eco-Environmental Sciences, Chinese Academy of Sciences. Published by Elsevier B.V.

The optimized g-C_3N_4–SNPs–*R. palustris* achieves remarkable PHB production titer of 3.19 ± 0.03 g L^{-1} with 11.79 %± 0.93 % quantum efficiency using solely CO_2 and SNPs.

A homogeneously autotrophic K/O co-doped g-C_3N_4 (K/O-CN) and *R. eutropha* biohybrid system has been reported for visible-light driven PHB production from CO_2 as shown in Figure 30(A).[126] This system introduces nano-sized, scattered rod-like K/O co-doped g-C_3N_4 (K/O-CN) as a replacement for bulk g-C_3N_4, therefore increasing the interface contact and mass transfer at the abiotic–biotic interface *R. eutropha* is accomplished.

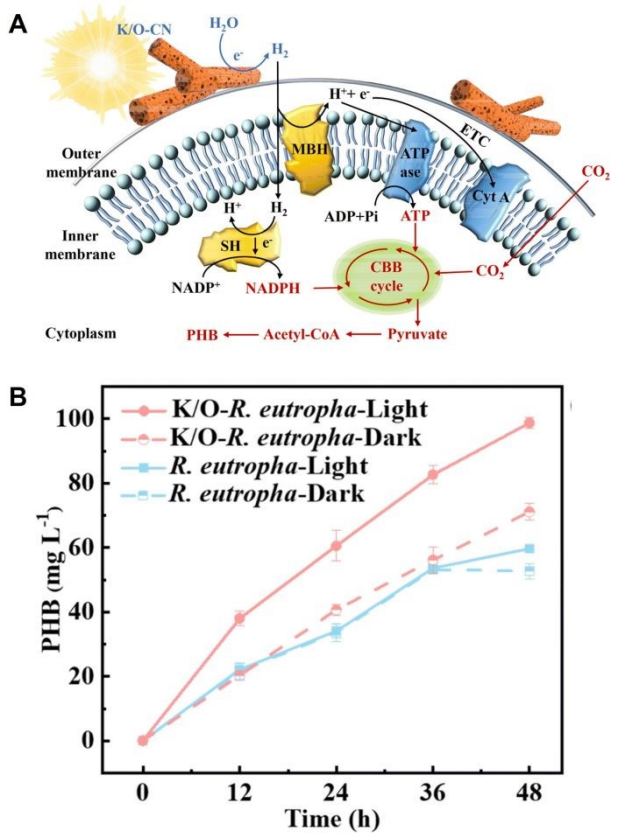

Fig. 30. Schematic representation for the visible-light driven PHB production from CO_2 with the system of K/O-CN-*R. eutropha* (A). Time dependence of PHB production from CO_2 using the hybrid system of K/O-CN-*R. eutropha* under visible-light irradiation (B). Reproduced with permission from ref 126. Copyright 2026 The Royal Society of Chemistry.

Figure 30(B) shows the time dependence of PHB production with the system of K/O-CN-*R. eutropha* under visible-light irradiation with light at an intensity of 4000 lux (0.75 mW cm^{-2}). A gas mixture (N_2 : H_2 : CO_2 : O_2 = 76 : 10 : 10 : 4) is used as carbon sources for this system. As shown in Figure 30(B), the K/O-CN–*R. eutropha* biohybrid achieves a PHB yield of 49.35 ± 0.85 mg L^{-1} day^{-1} surpassing non-metal-based biohybrids with adding co-factors and reaches a quantum efficiency of 5.88 ± 0.16% exceeding most metal-based biohybrid systems. By using K/O-CN–*R. eutropha*, the PHB production is improved compared to the dark condition or the system excluding K/O-CN.

Nanosheet composed of g-C_3N_4 is one of the promising visible light-responsive photocatalysts.[127] The g-C_3N_4 nanosheet (CNNS)-*R. eutropha* has been reported for visible-light driven PHB production from CO_2 as shown in Figure 31(A).[128]

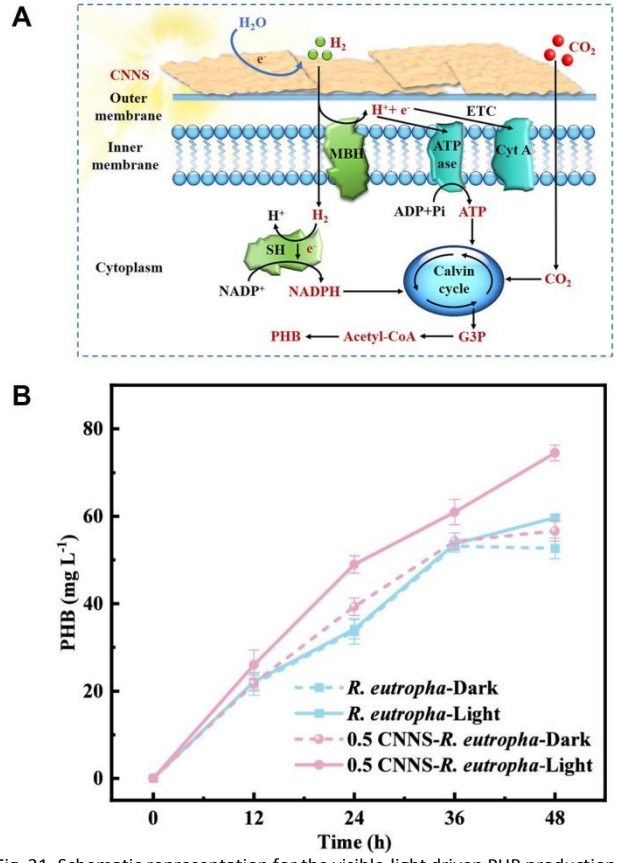

Fig. 31. Schematic representation for the visible-light driven PHB production from CO_2 with the system of CNNS -*R. eutropha* (A). Time dependence of PHB production from CO_2 using the hybrid system of CNNS -*R. eutropha* under visible-light irradiation (B). Reproduced with permission from ref 128. Copyright 2025 American Chemical Society.

Figure 31(B) shows the time dependence of PHB production with the system of CNNS -*R. eutropha* under continuous irradiation set to an intensity of 4000 lx. A gas mixture (N_2 : H_2 : CO_2 : O_2 = 76 : 10 : 10 : 4) is used as carbon sources for this system. Comparative experiments are conducted under both light and dark conditions as shown in Figure 31(B). The CNNS-*R. eutropha* system exhibits the highest PHB yield of 37.25 ± 0.9 mg·L^{-1}·day^{-1} under irradiation with 0.5 g L^{-1} CNNS, reflecting a 41.47% increase compared to the only *R. eutropha* under dark conditions (26.33 mg·L^{-1} day^{-1}). Thus, PHB production yield also surpasses the yields observed under both light and dark conditions without CNNS. Under dark conditions, the PHB yield is similar whether or not CNNS is added. This result indicates that CNNS dose not exert toxic effects on *R. eutropha*, and the

enhancement in PHB production within this system is light-dependent.

Let's focus on the photocatalyst in the hybrid system of photocatalysts and microbial cells introduced in this section. The photocatalysts used in hybrid systems are visible light-responsive semiconductors, and most of them have a proven track record in hydrogen production based on the photolysis of water. In hybrid systems, efficient electron and proton transfer from the photocatalyst to the microbial cell governs the CO_2 conversion rate. Therefore, developing catalysts that bring semiconductor photocatalysts into contact with the surface of microbial cells is a crucial key to achieving efficient CO_2 conversion.

Next, the separation of products based on CO_2 conversion using hybrid systems will be discussed. Currently, the products from the hybrid systems described in this section are only separated by high-performance liquid chromatography (HPLC). In addition, since microbial cells are used, suppressing by-products is another challenge for scaling up this system.

Visible-light driven 3-hydoroxybutylate production from CO_2 and acetone with the photocatalytic dye and cell extract including multi-enzyme hybrid system

Another visible-light driven production of biodegradable polymer precursor from CO_2 method is to use a cell extract containing crude enzymes as shown in Figure 32 instead of the microbial cell shown in Figure 5(b).

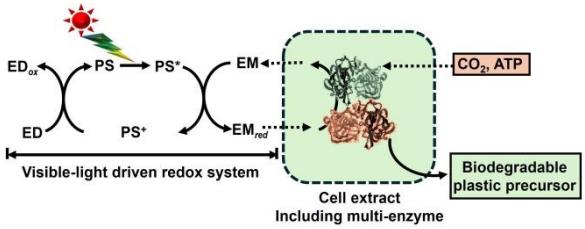

Fig. 32. Visible-light driven production of biodegradable plastic precursor based on the CO_2 fixation using hybrid system of photoredox consisting of ED, PS, and EM and a cell-extract containing crude enzymes.

This section describes the production of 3-hydroxybutyrate, a precursor of PHB, a promising biodegradable plastic. The research example on visible-light driven 3-hydroxybutyrate production with acetone carboxylase (AC; EC 6.4.1.6) and 3-hydroxybutyrate dehydrogenase (HBDH; EC 1.1.1.30) added as a catalyst in Figure 32 is introduced. Figure 33 shows the AC-catalyzed acetoacetate production from acetone and bicarbonate in the presence of ATP (a) and HBDH-catalyzed 3-hydroxybutyrate production based on the acetoacetate reduction in the presence of NADH (b). By using a dual-enzyme consisting of AC and HBDH, 3-hydroxybutyrate can be produced from acetone and bicarbonate via acetoacetate as an intermediate.[129,130]

Visible-light driven 3-hydroxybutylate production from bicarbonate or CO_2 and acetone with the system of TEOA, zinc tetraphenylporphyrin tetrasulfonate ($ZnTPPS^{4-}$; chemical structure is shown in Figure 34(a)), rhodium coordination complex ($[RhCp^*(bpy)(H_2O)]^{2+}$; Cp* = pentamethylcyclopentadienyl, bpy = 2,2'-bipyridyl; chemical structure is shown in Figure 34(b)), NAD^+, ATP, AC and HBDH has been reported.[131,132]

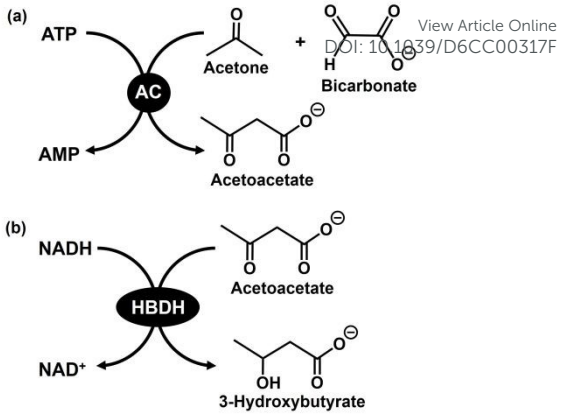

Fig. 33. AC-catalyzed acetoacetate production from acetone and bicarbonate in the presence of ATP (a). HBDH-catalyzed 3-hydroxybutyrate production based on the reduction of acetoacetate in the presence of NADH (b).

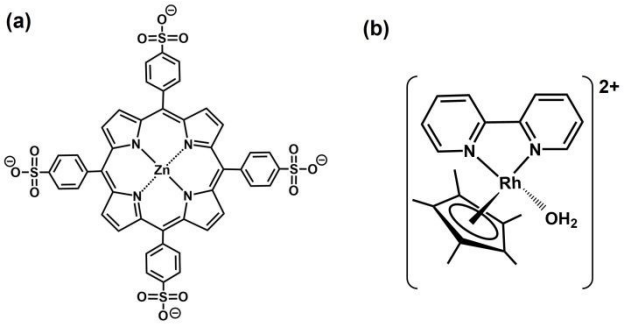

Fig. 34. Chemical structures of $ZnTPPS^{4-}$ (a) and $[RhCp^*(bpy)(H_2O)]^{2+}$(b).

AC[133, 134] and HBDH[130] are expressed from photosynthetic bacteria *Rhodobacter capsulatus* SB1003 (*Rb. capsulatus* SB1003) cultured in acetone-bicarbonate medium. The cell extract containing AC and HBDH is obtained from *Rb. capsulatus* SB1003. First, visible-light driven 3-hydroxybutyrate production from acetone and bicarbonate instead of CO_2 gas with the system of TEOA, $ZnTPPS^{4-}$, $[RhCp^*(bpy)(H_2O)]^{2+}$, NAD^+, ATP, cell extract containing AC and HBDH is introduced.[131] After 5 h irradiation with 250 W Halogen lamp ($\lambda > 390$ nm), 379 μM of 3-hydroxybutyrate is produced in the sample solution of acetone (0.5 mM), TEOA (0.2 M), $ZnTPPS^{4-}$ (50 μM), $[RhCp(bpy)(H_2O)]^{2+}$ (5.0 μM), NAD^+ (2.0 mM), sodium bicarbonate (50 mM), ATP (2.0 mM), magnesium chloride (5.0 mM) and cell extract (AC 0.051 U, HBDH 0.47 U) in 5.0 mL of 500 mM HEPES–NaOH buffer (pH 7.0). By using this system, *ca.* the conversion yield of acetone to 3-hydroxybutyrate is up to be approximately 76%.

Visible-light driven 3-hydroxybutyrate production from acetone and direct captured CO_2 from a mixture of N_2 and CO_2 gases with the system of TEOA, $ZnTPPS^{4-}$, $[RhCp(bpy)(H_2O)]^{2+}$, NAD^+, ATP and enzyme extract containing AC and HBDH is introduced.[132] Figure 35 shows the time dependence of acetoacetate (a) and 3-hydroxybutyrate (b) concentration in the sample solution of acetone (0.5 mM), TEOA (0.2 M), $ZnTPPS^{4-}$ (50 μM), $[RhCp(bpy)(H_2O)]^{2+}$ (5.0 μM), NAD^+ (2.0 mM), ATP (2.0 mM), magnesium chloride (5.0 mM) and cell extract (AC 0.062 U, HBDH 0.7 U) in 5.0 mL of 500 mM HEPES–NaOH buffer (pH 7.0) under conditions with varying ratios of

CO_2 and N_2 in the gas phase with irradiation with 250 W Halogen lamp (λ > 390 nm).

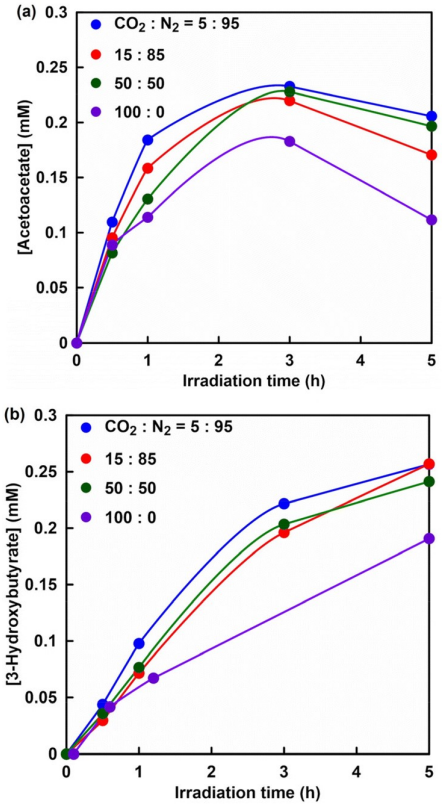

Fig. 35. Time dependence of acetoacetate (a) and 3-hydroxybutyrate (b) concentration in the sample solution of acetone, TEOA, $ZnTPPS^{4-}$, $[RhCp(bpy)(H_2O)]^{2}$, NAD^+, ATP, magnesium chloride and cell extract (AC, HBDH) in HEPES–NaOH buffer (pH 7.0) under conditions. with varying ratios of CO_2 and N_2 in the gas phase with irradiation Reproduced with permission from ref 132. Copyright 2023 The Royal Society of Chemistry.

The results using this system are summarized shown in Table 1. The data in Table 1 are calculated from figures published in reference 132.

Table 1. Concentration of 3-hydroxybutylate produced and conversion yield for acetone to 3-hydroxybutylate in the solution containing acetone, TEOA, $ZnTPPS^{4-}$, $[RhCp^*(bpy)(H_2O)]^{2+}$, NAD^+, ATP, magnesium chloride and cell extract containing AC and HBDH using mixture gas with various ratio of CO_2 and N_2 ($[CO_2/N_2]$) after 5 h visible light irradiation.

$[CO_2]/[N_2]$	[3-Hydroxybutyrate] (μM) after 5 h irradiation	Conversion yield for acetone to 3-hydoxybutyrate after 5 h irradiation %
0	0	0
0.05	257	51.4
0.15	257	51.4
0.5	241	48.2
1.0	190	38.0

As shown in Table 1, no significant difference in 3-hydroxybutyrate production is observed in the mixed gas with the ratio of CO_2 to N_2 not exceeding 0.5. In contrast, 3-hydroxybutyrate production decreases under the condition with 100% CO_2 gas compared to other conditions. The reason for this is presumed to be that the reaction system is isochoric and CO_2 in the gas phase dissolves into the sample solution and the pressure decreases as shown in Table 1. Under the condition of 100% CO_2, especially, it is predicted that the catalytic activity of cell extract involving AC and HBDH is inhibited based on the decrease in the pressure in the reaction system during the irradiation. Therefore, gaseous CO_2 can be directly used as a raw material without using bicarbonate, because of the gas-phase low concentration gaseous CO_2 trapping function of the HEPES-NaOH buffer solution used in the reaction. In addition, the captured gaseous CO_2 is converted to bicarbonate in the HEPES-NaOH buffer and acts as a carboxylating agent for acetone with an enzyme extract including AC. This suggests that a several to 20% of the gaseous CO_2 contained in gases emitted from thermal power stations, steel mills and chemical plants[142] could be used as feedstock in this system.

Finally, waste acetone and low-concentration CO_2 are applied to be used as raw materials in the visible-light driven 3-hydroxybutyrate production with the system of TEOA, $ZnTPPS^{4-}$, $[Cp^*Rh(bpy)(H_2O)]^{2+}$, NAD^+, ATP and cell extract including AC and HBDH.[137] Acetone is an abundant and useful chemical in the laboratory because it serves as a non-halogenated organic solvent that is miscible with water.[143] Acetone is relatively cheap, reasonably harmless and is often the solvent of choice in chemical laboratories for cleaning glassware contaminated with organic deposits. While acetone is useful as a solvent, it also requires a useful method of recycling after use. Because black permanent marker ink contains various organic solvents such as the *m*-xylene, *iso*-butanol, resin and oil soluble dyestuff, it can be used as a model for insoluble stains. The commercial black permanent marker ink used in this experiment contains 58% *m*-xylene, 14% *iso*-butanol, 16% resin and 12% oil soluble dyestuff. Here, black permanent marker ink dissolved in acetone is used as a waste solvent model. After adding the waste acetone to the HEPES buffer, the supernatant is separated from the precipitate, and the supernatant including acetone, *m*-xylene and *iso*-butanol is used for the visible-light driven 3-hydroxybutyrate production. The reaction mixture consists of supernatant including acetone (0.5 mM), ATP・2Na (2.0 mM), magnesium chloride (5.0 mM), TEOA (0.2 M), $ZnTPPS^{4-}$ (50 μM), $[RhCp^*(bpy)(H_2O)]^{2+}$ (5.0 μM), NAD^+(2.0 mM) and cell extract (AC: 0.062 U and HBDH: 0.7 U) with a mixed gas of a CO_2 to N_2 ratio of 0.15 in 5 mL of 500 mM HEPES-NaOH buffer. Figure 36 shows the time dependence of acetoacetate and 3-hydroxybutyrate concentration in the sample solution during irradiation with 250 W Halogen lamp (λ > 390 nm).

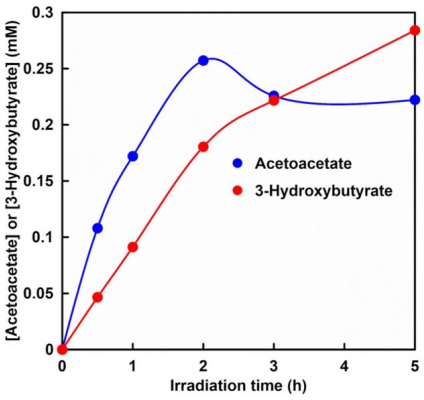

Fig. 36. Time dependence of acetoacetate or 3-hydroxybutyrate concentration in the solution of the supernatant containing acetone, ATP, magnesium chloride, TEOA, $ZnTPPS^{4-}$, $[RhCp (bpy)(H_2O)]^{2}$, NAD^+ and the cell extract (AC and HBDH:) in HEPES–NaOH buffer under conditions with a mixed gas of a CO_2 to N_2 ratio of 0.15 in the gas phase with irradiation. Reproduced with permission from ref 132. Copyright 2023 The Royal Society of Chemistry.

After 5 h irradiation, 0.28 mM of 3-hydroxybutyrate is produced. No significant difference is observed between pure and waste acetone in the visible-light driven 3-hydroxybutyrate synthesis using low concentrations of gaseous CO_2.

Strategy for visible-light driven production of CO_2-based biodegradable plastic precursors with photocatalytic dye and multi-enzyme hybrid system

The method of directly using microbial cells as a biocatalyst has the advantages of being simple and high in product yield, but it also has the drawback of being difficult to control the selectivity of the target product. Therefore, it has been proposed to produce biodegradable plastic precursors by incorporating an enzyme (ENZ) with the function of CO_2 fixation into a photoredox system consisting of an electron donor (ED), a visible light sensitizer (PS), and an electron mediator (EM) as shown in Figure 37.[135-137]

By incorporating hydrogenase (H_2ase; EC 1.12.2.1; cytochrome-c_3 hydrogenase,[143-148] EC 1.12.7.2; ferredoxin hydrogenase[145-150]) and formate dehydrogenase[151-155] (FDH; EC 1.17.1.9; NAD^+-dependent, EC 1.17.1.10; $NADP^+$-dependent, and EC 1.17.98.4; selenium-containing formate dehydrogenase H) into a photoredox system consisting of ED, PS, and EM, visible light-driven hydrogen production and formate production based on CO_2 reduction have been achieved.

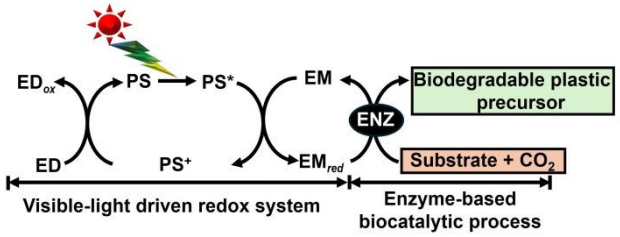

Fig. 37. Visible-light driven production of biodegradable plastic precursor based on the CO_2 fixation to a substrate with the system of an electron donor (ED), a visible-light sensitizer (PS), an electron mediator (EM) and an enzyme (ENZ).

The first example of applying this system to fixation of CO_2 to a substrate is shown in Figure 38.[151]

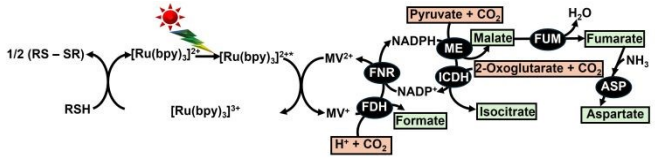

Fig. 38. Visible-light driven CO_2 fixation with the photoredox system of 2-mercaptoethanol (RSH), tris(2,2'-bipyridyl)ruthenium(II) ($[Ru(bpy)_3]^{2+}$) and methyl viologen (MV^{2+}) linked enzymes. FNR: ferredoxin-$NADP^+$ reductase, ICDH: isocitrate dehydrogenase, FUM: fumarase, ASP: L-aspartase

In this system, $[Ru(bpy)_3]^{2+}$ (chemical structure is shown in Figure 39) is used as the PS.

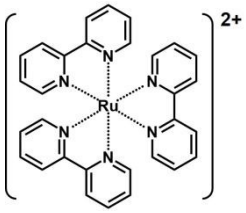

Fig. 39. Chemical structure of tris(2,2'-bipyridyl)ruthenium(II) ($[Ru(bpy)_3]^{2+}$).

As shown in Figure 38, FDH (EC 1.12.2.1), ICDH (EC 1.1.1.42), and ME (EC 1.1.1.40) can be used as CO_2 conversion enzymes in the photoredox system. When FDH is used as the enzyme in a photoredox system, the $MV^{\cdot+}$ can be used directly as a coenzyme instead of NAD(P)H. On the other hand, when ICDH or ME is used as an enzyme in a photoredox system, it is necessary to incorporate NADPH regeneration. In Figure 38, the biodegradable plastic precursors malate, fumarate, and aspartate are produced using CO_2 as a raw material by a photoredox system incorporating enzymes. Polymers derived from malate or aspartate precursors are biodegradable as shown in Figure 40.

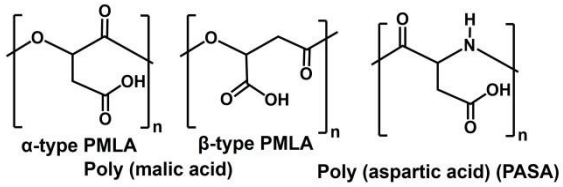

Fig. 40. Chemical structures of poly (malic acid)[157-159] and poly (aspartic acid)[160,161].

Fumarate can also be used as a precursor to the biodegradable plastic PBS. For the first time, a system incorporating ME, FUM (EC 4.2.1.2), and ASP (EC 4.3.1.1) as catalysts in a photoredox system of RSH, $[Ru(bpy)_3]^{2+}$, MV^{2+}, FNR (EC 1.18.1.2) and $NADP^+$ has been successfully used to produce fumarate and aspartate from CO_2 and pyruvate under visible-light irradiation. Figure 41 shows the time dependence of fumarate (a) and aspartate (b) production with the system of RSH (16 mM), $[Ru(bpy)_3]^{2+}$ (23 μM), MV^{2+} (0.16 mM), $NADP^+$(0.32 mM), pyruvic acid (40 mM), sodium bicarbonate (0.16 M), ammonium ion (80 mM), manganese chloride (80 μM), FNR (0.5 U), ME (0.5 U), FUM (156 U) and ASP (3.0 U) in 4.0 mL of 0.16 M Tris-buffer solution (pH 7.9) during visible-light irradiation (1000 W halogen quartz lamp with 400 nm cut-off filter).

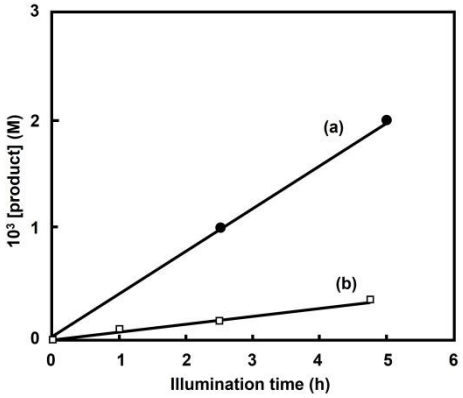

Fig. 41. Time dependence of concentration of aspartate (a) and fumarate (b) production with the system of RSH, $[Ru(bpy)_3]^{2+}$, MV^2, $NADP^+$, pyruvic acid, sodium bicarbonate, ammonium ion, manganese chloride, FNR, ME, FUM and ASP in Tris-buffer solution during visible-light irradiation. Reproduced with permission from ref 156. Copyright 1988 The Royal Society of Chemistry.

As shown in Figure 41, fumarate and aspartate production are increased during visible-light irradiation. After 5 h irradiation, *ca*. 1.3 and 2.0 mM of fumarate and aspartate are produced. In the absence of ASP, no aspartate is produced and malate and fumarate are produced during visible-light

irradiation. Also, visible-light driven malate production with the system of RSH (19 mM), $[Ru(bpy)_3]^{2+}$ (21 μM), MV^{2+} (0.19 mM), $NADP^+$(0.18 mM), pyruvic acid (47 mM), sodium bicarbonate (0.20 M), manganese chloride (95 μM), FNR (0.2 U) and ME (1.33 U) in 4.2 mL of 0.20 M Tris-buffer solution (pH 7.9) under a gaseous atmosphere of CO_2 during visible-light irradiation (1000 W halogen quartz lamp with 400 nm cut-off filter). After 2 h irradiation, 3.0 mM of malate production is observed.[156]

Thus, in order to produce biodegradable plastic precursors such as malate, fumarate, and aspartate, it is essential to develop a visible-light-driven NAD(P)H regeneration system consisting of ED, PS, EM, and a catalyst that can be linked to an enzyme-based biocatalytic process. Visible light-driven NAD(P)H regeneration, consisting of ED, PS, EM, and a catalyst, has been extensively studied in two main systems (Figure 42).[135-137] The first is a visible light-driven NADPH regeneration system using FNR as a catalyst (Figure 42(a)). The other is a visible light-driven NAD(P)H regeneration system using $([RhCp^*(bpy)(H_2O)]^{2+}$ as a catalyst (Figure 42(b)). In the system shown in Figure 42(a), visible-light driven NADPH regeneration systems using $[Ru(bpy)_3]^{2+}$,[156] 5-deazariboflavin,[162] riboflavin,[162] proflavin,[162,161] oligothiophene derivatives,[164] CdS,[165] CdSe quantum dots[166] and polyethylene glycol modified chlorophyll-*a* (PEG-Chl-*a*)[167] as PSs have been reported. In addition to 4,4'-bipyridinium salts such as MV^{2+}, 2,2'-bipyridinium salts and ferredoxin are used as EMs in this system.[163] In the system of Figure 42 (b), on the other hand, visible-light driven NAD(P)H regeneration systems using carbon-doped TiO_2,[168] phosphate-doped TiO_2,[169] eosin-Y,[170] porphyrin derivatives[171,172] and proflavine[173] as PSs have been reported. Research examples on visible light-driven NAD(P)H regeneration systems have been summarized and reported in several reviews.[135-137, 174, 175]

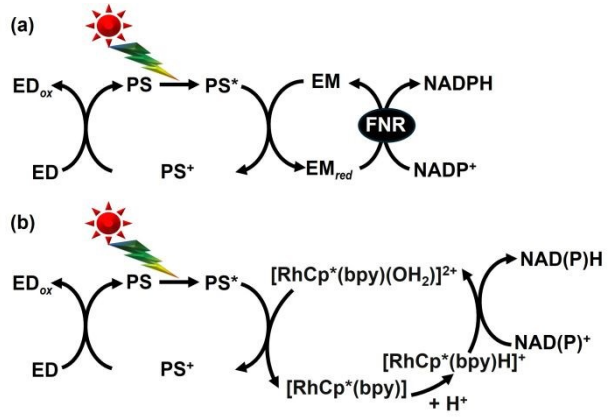

Fig. 42. Visible-light driven NAD(P)H regeneration with the system of ED, PS, EM and FNR (a) and with the system of ED, PS, $[RhCp^*(bpy)(H_2O)]^{2+}$ (b).

The strategy for visible light-driven CO_2-based biodegradable plastic precursor production using a photocatalytic dye and multi-enzyme hybrid system involves the integrated coupling of an NAD(P)H regeneration system and an enzyme-based biocatalytic process.

Visible-light driven malate production with photocatalytic dye and enzyme hybrid system

As mentioned above, visible-light driven malate production from CO_2 and pyruvate has been achieved using system of RSH, $[Ru(bpy)_3]^{2+}$, MV^{2+}, $NADP^+$, FNR and ME has been developed for the first time. Some studies have been reported on the production of malate using visible light-driven NADPH regeneration catalyzed by FNR in the presence of ME.

Visible-light driven malate production from CO_2 and pyruvic acid (2.0 mM) with the system of RSH (27 mM), CdS or TiO_2 microcrystals fixed in the interlayer spacings of sodium montmorillonite (TiO_2/clay) (1.25 mM) as a PS, MV^{2+} (1.0 mM), $NADP^+$ (0.1 mM), FNR (0.2 U) and ME (1.0 U) in CO_2-saturated Tris-buffer (10 mL) has been reported.[175] For the system using CdS or TiO_2/clay, *ca.* 1.0 or 0.3 mM of malate is produced after 5 h irradiation with 500 W high-pressure Hg arc lamp, respectively.

Visible light-driven malate production using chlorophyll derivative, zinc chlorin e6 (ZnCe6; chemical structure is shown in Figure 43) as PS in the system shown in Figure 52(a) has also been reported.[176]

After 3 h irradiation with 250 W-W lamp (λ > 365 nm), 0.65 mM of malate production is observed with the system of NADH (3.0 mM), ZnCe6 (50 μM), MV^{2+} (1.0 mM), FNR (4.0 U), pyruvic acid (10 mM), sodium bicarbonate (10 mM), $NADP^+$ (10 mM) and ME (4.5 U) in 50 mM of Bis–Tris buffer (3.0 mL; pH 8.0).

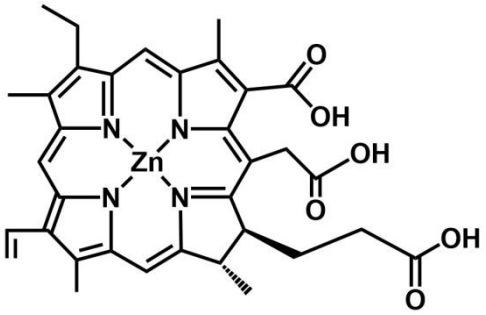

Fig. 43. Chemical structure of zinc chlorin e6 (ZnCe6).

It has been reported that NADPH can be regenerated even in the absence of MV^{2+} using PEG-Chl-*a* (chemical structure is shown in Figure 44) as PS in Figure 42(a).[167]

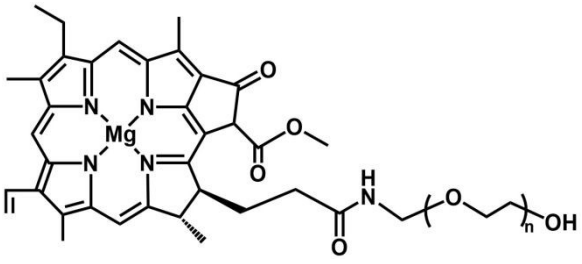

Fig. 44. Chemical structure of PEG-Chl-*a*.

By using PEG-Chl-*a* (15 μM) as a PS, malate production in the system of sodium ascorbate (6.0 mM), sodium bicarbonate (180 mM), magnesium chloride (15 mM), sodium pyruvate (0.8 mM), $NADP^+$ (3.2 mM), FNR (2.5 U) and ME (5.0 U) in 50 mM of phosphate buffer (10 mL; pH 7.4) during irradiation with a 60 W incandescent lamp from a distance of 10 cm (light intensity, 200 J $m^{-2}s^{-1}$) is observed and 0.15 mM of malate is produced after 4 h irradiation.

View Article Online
DOI: 10.1039/D6CC00317F

In addition, the optical activity of the malate produced in the reaction system introduced in this section, D- or L-, has not been identified.

Next, research example on visible-light driven malate production with ME added as a catalyst in Figure 42(b) is introduced. Visible-light driven L-malate production from sodium bicarbonate and pyruvate with the system of triethanol amine (TEOA) as ED, water-soluble zinc porphyrin, $ZnTPPS^{4-}$; as PS, $[RhCp^*(bpy)(H_2O)]^{2+}$, NAD^+, and ME is introduced.[177]

After 5 h irradiation with 250 W Halogen lamp (λ > 390 nm), 0.16 mM of L-malate production is observed with the system of sodium pyruvate (5.0 mM), TEOA (0.2 M), $ZnTPPS^{4-}$ (10 μM), $[RhCp^*(bpy)(H_2O)]^{2+}$ (10 μM), NAD^+ (0.5 mM), sodium bicarbonate (100 mM), magnesium chloride (5.0 mM) and ME (0.7 U) in CO_2-saturated 500 mM HEPES–NaOH buffer (5.0 mL; pH 7.3). On the other hand, 40 μM of L-malate production is observed under Ar-saturated 500 mM HEPES–NaOH buffer (pH 7.3). This result suggests that the equilibrium between gaseous CO_2 in the gas phase and bicarbonate ion in the sample solution is important for ME-catalysed L-malate production. In particular, this sealed isochoric system has the problem of a decrease in pressure within the system because gaseous CO_2 in the gas phase of the reaction vessel is captured by the weak basic buffer solution. Therefore, visible-light driven L-malate production has also been reported using an isobaric reaction system attached balloon filled with 1 L of CO_2 gas.[178] After 5 h irradiation with 250 W Halogen lamp (λ > 390 nm), *ca*. 0.16 mM of L-malate production is observed with the system of sodium pyruvate (5.0 mM), TEOA (0.2 M), $ZnTPPS^{4-}$ (10 μM), $[RhCp^*(bpy)(H_2O)]^{2+}$ (10 μM), NAD^+ (0.5 mM), magnesium chloride (5.0 mM) and ME (0.7 U) in 500 mM HEPES–NaOH buffer (5.0 mL; pH 7.3). A balloon filled with 1 L of CO_2 gas is attached to the reaction vessel, and the pressure inside the reaction system is maintained at 1.0 atm. Furthermore, no sodium bicarbonate is added to the reaction sample. The increase in L-malate over the irradiation time indicates that bicarbonate is continuously captured from CO_2 gas and fixed to pyruvate by ME together with NADH regenerated by visible light irradiation. By using this isobaric system, L-malate can be produced directly using gaseous CO_2 as a raw material.

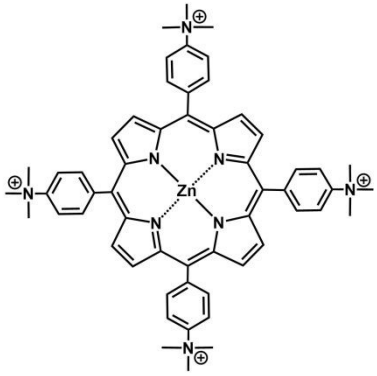

Fig. 45. Chemical structure of $ZnTMAP^{4+}$.

In addition, visible light-driven L-malate production using a water-soluble cationic zinc porphyrin, zinc tetrakis(4-*N,N,N*-trimethylaminophenyl)porphyrin ($ZnTMAP^{4+}$; chemical structure is shown in Figure 45) as a PS has also been reported.[179]

After 5 h irradiation with 250 W Halogen lamp (λ > 390 nm), *ca*. 0.25 mM of L-malate production is observed with the system of sodium pyruvate (5.0 mM), TEOA (0.2 M), $ZnTMAP^{4+}$ (50 μM), $[RhCp^*(bpy)(H_2O)]^{2+}$ (10 μM), NAD^+ (0.5 mM), magnesium chloride (5.0 mM) and ME (0.7 U) in 500 mM HEPES–NaOH buffer (5.0 mL; pH 7.3). A balloon filled with 1 L of CO_2 gas is attached to the reaction vessel, and the pressure inside the reaction system is maintained at 1.0 atm. By using $ZnTMAP^{4+}$ as a photosensitiser, approximately 1.5 times more L-malate is produced than in the system with $ZnTPPS^{4-}$. As a stable NAD^+ reduction NADH in a system of TEOA and $[Cp^*Rh(bpy)(H_2O)]^{2+}$ with $ZnTMAP^{4+}$ as a PS compared to a system using $ZnTPPS^{4-}$, thus, the efficiency of visible-light driven L-malate production is improved by using $ZnTMAP^{4+}$.

As described above, L-malate production from CO_2 and pyruvate using ME as a photoredox catalyst has been achieved. However, in the production of L-malate using ME as a catalyst, L-lactate is produced through the reduction of pyruvate under low concentration of CO_2 or bicarbonate. Therefore, a system mimicking the mitochondrial pyruvate malate shuttle,[180,181] consisting of pyruvate carboxylase (PC; EC 6.4.1.1) and malate dehydrogenase (MDH; EC 1.1.1.37) in the presence of ATP and NADH, has been proposed for the purpose of producing L-malate using low-concentration CO_2 as a feedstock.

Figure 46 shows the PC-catalyzed oxaloacetate production from pyruvate and bicarbonate in the presence of ATP (a) and MDH-catalyzed L-malate production based on the oxaloacetate reduction in the presence of NADH (b). By using a dual-enzyme consisting of PC and MDH, L-malate can be produced from pyruvate and bicarbonate via oxaloacetate as an intermediate. In addition, by using PC as a catalyst, no reduction process of pyruvate is involved to suppresses L-lactate production and enables the use of low-concentration CO_2 as a raw material.[182,183]

Fig. 46. PC-catalyzed oxaloacetate production from pyruvate and bicarbonate in the presence of ATP (a). MDH-catalyzed L-malate production based on the reduction of oxaloacetate in the presence of NADH (b).

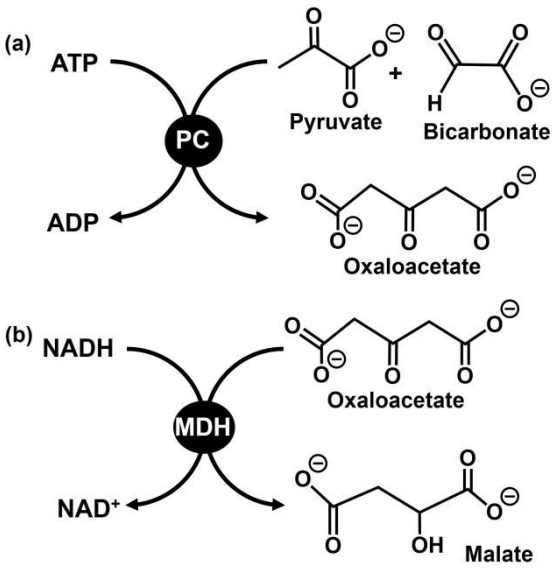

Visible-light driven L-malate production from pyruvate and CO_2 with the system of TEOA, $ZnTMAP^{4+}$, $[RhCp^*(bpy)(H_2O)]^{2+}$, NAD^+, ATP, acetyl-CoA, PC and MDH has been reported.[184] Figure 47 shows the time dependence of L-malate production with the system of sodium pyruvate (5.0 mM), acetyl-CoA (1.0 mM), magnesium chloride (5.0 mM), sodium ATP (5.0 mM), TEOA (0.2 M), $ZnTMAP^{4+}$ (50 μM), NAD^+ (5.0 mM), $[RhCp^*(bpy)(H_2O)]^{2+}$ (0.1 mM), PC (1.0 U) and MDH (20 U) in 5.0 mL of 500 mM HEPES-NaOH buffer solution (pH 7.8) under visible-light irradiation with 250 W Halogen lamp (λ > 390 nm). A balloon filled with 1 L of mixture gas of N_2 and CO_2 is attached to the reaction vessel, and the pressure inside the reaction system is maintained at 1.0 atm. As shown in Figure 47, more L-malate production is observed under 15.0% CO_2 condition than under 100% CO_2. The change in pH of the sample solution during the reaction is measured, and the pH is dropped from 7.8 to 7.0 under 100% CO_2 condition. On the other hand, no change in pH of the sample solution during reaction under 15.0% CO_2 condition is observed. It has been reported that the rate of visible-light driven NADH regeneration decreases as the pH of the sample solution decreases. Therefore, the low L-malate production under 100% CO_2 condition is due to a decrease in NADH regeneration induced by a drop in pH during irradiation. By complementing the catalytic function of ME with PC and MDH, visible-light driven L-malate production using low-concentration CO_2 as a direct feedstock is accomplished.

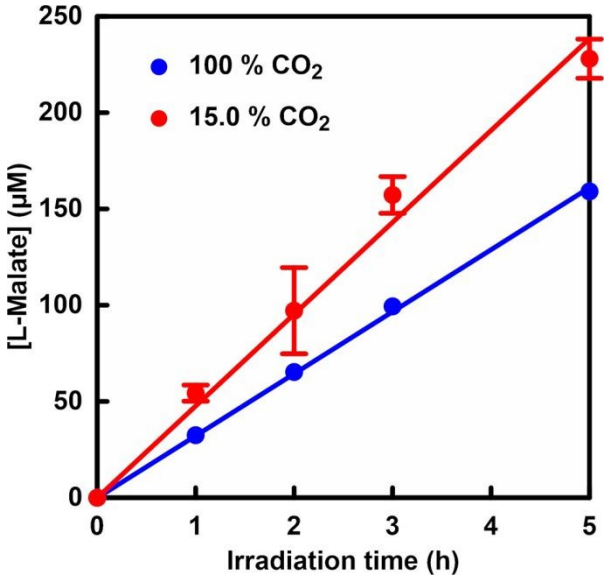

Fig. 47. Time dependence of L-malate production in the system of sodium pyruvate, acetyl-CoA, magnesium chloride, sodium ATP, TEOA, $ZnTMAP^{4+}$, NAD^+, $[Rh Cp^*(bpy)(H_2O)]^2$, PC and MDH in HEPES-NaOH buffer solution (pH 7.8) under visible-light irradiation. The gas phase of the reaction vessel was introduced with 15.0 (red) or 100% CO_2 (blue) gas. Reproduced with permission from ref 184. Copyright 2025 American Chemical Society.

Finally, an overview of the visible-light driven L-malate production from CO_2 and pyruvate using photocatalytic dye and enzyme hybrid system reviewed in this section is summarized in Table 2.

Visible-light driven fumarate production from CO_2 and pyruvate with the photocatalytic dye and enzyme hybrid system

Malate is a precursor to PMLA, but can be converted by dehydration to fumarate, a precursor to a more versatile biodegradable plastic. In other words, by incorporating FUM in addition to ME, fumarate can be produced from CO_2. The production of fumarate from CO_2 as a raw material by hybridising a visible-light driven NADH regeneration system consisting of a photocatalytic dye and a catalyst with dual-enzyme consisting of ME and FUM is introduced in this section.

Table 2. Summary of the visible-light driven malate production from carbonate species and pyruvate using photocatalytic dye and enzyme hybrid system

System	Malate production (mM)	Ref
RSH (19 mM), $[Ru(bpy)_3]^{2+}$ (21 μM), MV^{2+} (0.19 mM), $NADP^+$(0.18 mM), pyruvic acid (47 mM), sodium bicarbonate (0.20 M), manganese chloride (95 μM), FNR (0.2 U) and ME (1.33 U)	1.5	156
RSH (27 mM), CdS or TiO_2/clay (1.25 mM), MV^{2+} (1.0 mM), $NADP^+$ (0.1 mM), pyruvic acid (2.0 mM), FNR (0.2 U) and ME (1.0 U) in CO_2 saturated buffer	0.2 for CdS 0.06 for TiO_2/clay	175
NADH (3.0 mM), ZnCe6 (50 μM), MV^{2+} (1.0 mM), FNR (4.0 U), pyruvic acid (10 mM), sodium bicarbonate (10 mM), $NADP^+$ (10 mM) and ME (4.5 U)	0.21	162
sodium ascorbate (6.0 mM), PEG-Chl-*a* (15 μM), sodium bicarbonate (180 mM), magnesium chloride (15 mM), sodium pyruvate (0.8 mM), $NADP^+$ (3.2 mM), FNR (2.5 U) and ME (5.0 U)	0.0375	167
sodium pyruvate (5.0 mM), TEOA (0.2 M), $ZnTPPS^{4-}$ (10 μM), $[RhCp^*(bpy)(H_2O)]^{2+}$ (10 μM), NAD^+ (0.5 mM), sodium bicarbonate (100 mM), magnesium chloride (5.0 mM) and ME (0.7 U) in CO_2-saturated buffer	0.032	177
sodium pyruvate (5.0 mM), TEOA (0.2 M), $ZnTPPS^{4-}$ (10 μM), $[RhCp^*(bpy)(H_2O)]^{2+}$ (10 μM), NAD^+ (0.5 mM), magnesium chloride (5.0 mM) and ME (0.7 U) in CO_2-saturated buffer	0.032	178
sodium pyruvate (5.0 mM), TEOA (0.2 M), $ZnTMAP^{4+}$ (50 μM), $[RhCp^*(bpy)(H_2O)]^{2+}$ (10 μM), NAD^+ (0.5 mM), magnesium chloride (5.0 mM) and ME (0.7 U) in CO_2-saturated buffer	0.050	179
sodium pyruvate (5.0 mM), acetyl-CoA (1.0 mM), magnesium chloride (5.0 mM), sodium ATP (5.0 mM), TEOA (0.2 M), $ZnTMAP^{4+}$ (50 μM), NAD^+ (5.0 mM), $[RhCp^*(bpy)(H_2O)]^{2+}$ (0.1 mM), PC (1.0 U) and MDH (20 U)	0.23 (15% CO_2) 0.15 (100% CO_2)	184

As mentioned above, visible-light driven fumarate production from CO_2 and pyruvate has been achieved using system of RSH, $[Ru(bpy)_3]^{2+}$, MV^{2+}, $NADP^+$, FNR, ME and FUM. No other studies have been reported on the production of

fumarate using visible-light driven NADPH regeneration catalysed by FNR in the presence of ME and FUM.

First, visible-light driven fumarate production from pyruvate and bicarbonate instead of CO_2 gas by using the system of TEOA, $ZnTPPS^{4-}$, $[RhCp^*(bpy)(H_2O)]^{2+}$, NAD^+, ME and FUM is introduced.[172] The sample solution consists of TEOA (0.2 M), $ZnTPPS^{4-}$ (10 μM), $[RhCp^*(bpy)(H_2O)]^{2+}$ (10 μM), NAD^+ (0.5 mM), sodium pyruvate (5.0 mM), sodium bicarbonate (100 mM), magnesium chloride (5.0 mM), ME (0.7 U) and FUM (0.5 U) in 5.0 mL of CO_2-saturated 500 mM HEPES-NaOH buffer (5.0 mL; pH 7.8). The sample solution is irradiated with visible-light irradiation with 250 W Halogen lamp (λ > 390 nm). By using this system, the concentration of L-malate and fumarate are estimated to be 194 and 48 μM, respectively after 5 h irradiation. While the production of L-malate tends to reach a constant concentration, the fumarate concentration linearly increases during irradiation. Visible-light driven fumarate production has also been reported using an isobaric reaction system attached balloon filled with 1 L of CO_2 gas.[178] After 5 h irradiation with 250 W Halogen lamp (λ > 390 nm), *ca*. 190 and 49 μM of L-malate and fumarate production are observed with the system of sodium pyruvate (5.0 mM), TEOA (0.2 M), $ZnTPPS^{4-}$ (10 μM), $[RhCp^*(bpy)(H_2O)]^{2+}$ (10 μM), NAD^+ (0.5 mM), magnesium chloride (5.0 mM), ME (0.7 U) and FUM (0.5 U) in 500 mM HEPES–NaOH buffer (5.0 mL; pH 7.8). A balloon filled with 1 L of CO_2 gas is attached to the reaction vessel, and the pressure inside the reaction system is maintained at 1.0 atm. Furthermore, no sodium bicarbonate is added to the reaction sample. No significant difference in fumarate production is observed under 100% CO_2 in the gas phase and the presence of bicarbonate conditions. On the other hand, it has been reported that as the CO_2 ratio in the mixed gas in the balloon decreases, the production of L-malate and fumarate also decreases.

Using system of TEOA, $ZnTPPS^{4-}$, $[RhCp^*(bpy)(H_2O)]^{2+}$, NAD^+, ME and FUM, the concentration of fumarate produced remains significantly lower than that of L-malate, whether CO_2 gas or bicarbonate is used as the feedstock. For example, it has been reported that the addition of phosphate improves the catalytic activity of FUM for the production of fumarate based on the dehydration of L-malate.[185] In other words, anionic or cationic substances may control the catalytic activity of FUM. Thus, the effect of water-soluble zinc porphyrin on the FUM-catalysed dehydration of L-malate to produce fumarate has been investigated. The effects of water-soluble zinc porphyrins $ZnTPPS^{4-}$ and $ZnTMAP^{4+}$, as well as zinc tetra(4-carboxyphenyl)porphyrin ($ZnTCPP^{4-}$) and zinc tetrakis(4-methylpyridyl)porphyrin ($ZnTMPyP^{4+}$) on the enzyme activity of FUM for fumarate production. Figure 48 shows the chemical structures of $ZnTCPP^{4-}$ and $ZnTMPyP^{4+}$.

As shown in Figure 49, Addition of cationic zinc porphyrins, $ZnTMPyP^{4+}$ or $ZnTMAP^{4+}$, no fumarate production from L-malate by FUM is altered compared to control experiment. By addition of anionic zinc porphyrins, $ZnTCPP^{4-}$ or $ZnTPPS^{4-}$, in contrast, the fumarate production from L-malate with FUM is suppressed. Especially, the fumarate production with FUM is strongly inhibited in the presence of $ZnTPPS^{4-}$.

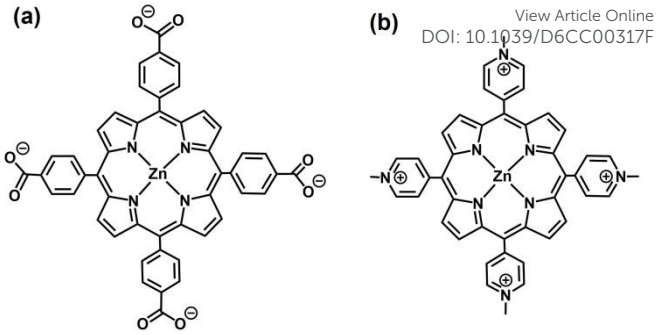

Fig. 48. Chemical structures of $ZnTCPP^{4-}$(a) and $ZnTMPyP^{4+}$ (b).

It is suggested that the sulfo-group bonded to the zinc porphyrin has a stronger effect on the catalytic activity of FUM than that of the carboxy-group.[186]

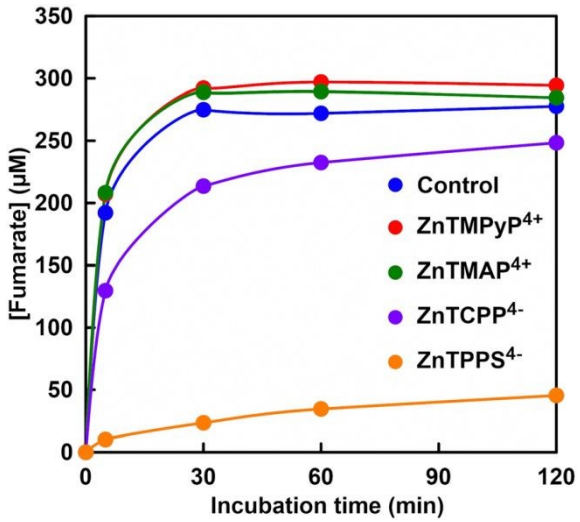

Fig. 49. Time dependence of fumarate production from L-malate with FUM in the presence of zinc porphyrin during incubation. Reproduced with permission from ref 185. Copyright 2023 The Royal Society of Chemistry.

Here, let us focus on the structural interactions between FUM and water-soluble zinc porphyrins. In the research presented in this session, FUM is an enzyme derived from porcine heart. The three-dimensional structures of porcine heart-derived and related FUMs have been reported.[187-189] It has been reported that porcine heart-derived FUM is composed of four subunits. FUM has four active sites (site A) with high affinity for substrates, as well as an additional binding site (site B) with low affinity for substrates.[189] Figure 50 is a schematic diagram showing the active high-affinity substrate binding sites (A) and low-affinity binding sites (B) in the FUM.

For example, tetracarboxylic acid, benzene-1,2,4,5-tetracarboxylate and sulfate have been reported as strong inhibitors for FUM.[189] In particular, it is found that one molecule of benzene-1,2,4,5-tetracarboxylic acid can bind to both sites A and B simultaneously, and that four carboxyl groups of benzene-1,2,4,5-tetracarboxylic acid per FUM molecule bind with high affinity, acting as bridges between the two subunits. These results suggest that the four benzenesulfonate groups of $ZnTPPS^{4-}$ also bind with high affinity to the substrate-binding

sites (sites A and B) of FUM, inhibiting the dehydration of L-malate and reducing the production of fumarate.

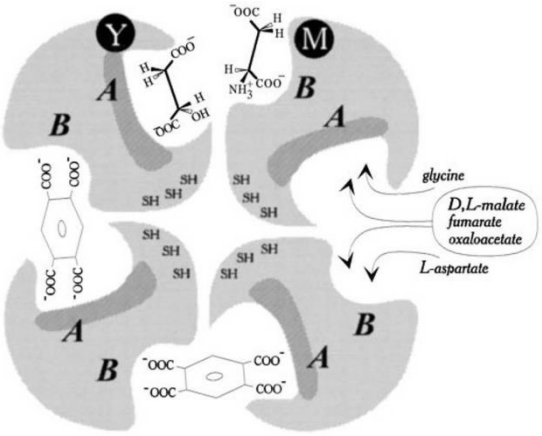

Fig. 50. Schematic representation showing the active high-affinity substrate binding sites (A) and low-affinity binding sites (B) in the FUM. Reproduced with permission from ref 189. Copyright 1998 ASBMB. Currently published by Elsevier Inc; originally published by American Society for Biochemistry and Molecular Biology. Creative Commons CC-BY-NC license.

Therefore, a visible-light driven fumarate production system has been reported that uses $ZnTMAP^{4+}$ as PS instead of $ZnTPPS^{4-}$, which does not affect FUM enzyme activity.[179] Visible-light driven fumarate production has also been reported using an isobaric reaction system attached balloon filled with 1 L of CO_2 gas.[179,190] After 5 h irradiation with 250 W Halogen lamp (λ > 390 nm), *ca*. 97 μM of fumarate production is observed with the system of sodium pyruvate (5.0 mM), TEOA (0.2 M), $ZnTMAP^{4+}$ (50 μM), $[RhCp^*(bpy)(H_2O)]^{2+}$ (10 μM), NAD^+ (0.5 mM), magnesium chloride (5.0 mM), ME (0.7 U) and FUM (0.5 U) in 500 mM HEPES–NaOH buffer (5.0 mL; pH 7.8). A balloon filled with 1 L of CO_2 gas is attached to the reaction vessel, and the pressure inside the reaction system is maintained at 1.0 atm. Figure 51 shows the fumarate concentration using $ZnTMAP^{4+}$ or $ZnTPPS^{4-}$ after 5 h irradiation.

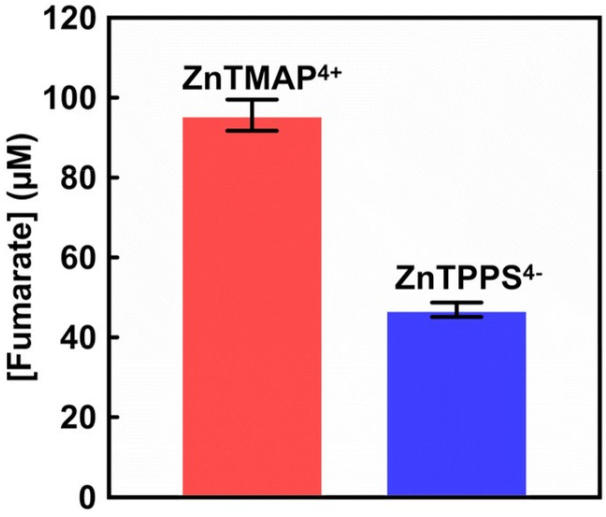

Fig. 51. The concentration of fumarate production in the system of sodium pyruvate, magnesium chloride, TEOA, $[RhCp^*(bpy)(H_2O)]^{2+}$, NAD^+, MDH, FUM and CO_2 gas in the presence of $ZnTMAP^{4+}$ (red) or $ZnTPPS^{4-}$ (blue) after 5 h irradiation. Reproduced with permission from ref 179. Copyright 2023 The Royal Society of Chemistry.

The efficiency of visible-light driven fumarate production from pyruvate and gaseous CO_2 by using $ZnTMAP^{4+}$ as a PS in the system combination of NAD^+ reduction with $[RhCp^*(bpy)(H_2O)]^{2+}$ and dual-biocatalyst consisting of MDH and FUM in the presence of TEOA is improved approximately 2.0 times more fumarate produced than in the system using $ZnTPPS^{4-}$, conventionally PS.

As a relevant study of this system, fumarate production from pyruvate and bicarbonate using a core-shell type of benzodiimidazole oligomer-$BaSO_4$ immobilised $[RhCp^*(bpy)(H_2O)]^{2+}$ (BaPP@BDO-Rh) instead of water-soluble zinc porphyrin as a visible-light sensitising material with dual-biocatalyst consisting of ME and FUM has been reported as shown in Figure 52(A).[191] In this study, ME and FUM are expressed in *E. coli* strain DE3 using the pET28a vector, and then the enzymes are purified for use in this reaction. The ME and FUM are designated as MaeB and FumC, respectively. The sample solution consists of TEOA (1.0 M), 1 g L^{-1} BaPP@BDO-Rh, NAD^+ (1.0 mM), sodium pyruvate (5.0 mM), sodium bicarbonate (100 mM), magnesium chloride (5.0 mM), MaeB (1.0 U) and FumC (1.0 U) in 3.0 mL of 100mM phosphate buffer. The sample solution is irradiated with 100 W xenon lamp at room temperature as a visible light source. By using this system, the concentration of L-malate and fumarate are estimated to be 114 and 63 μM, respectively after 1 h irradiation as shown in Figure 52(B).

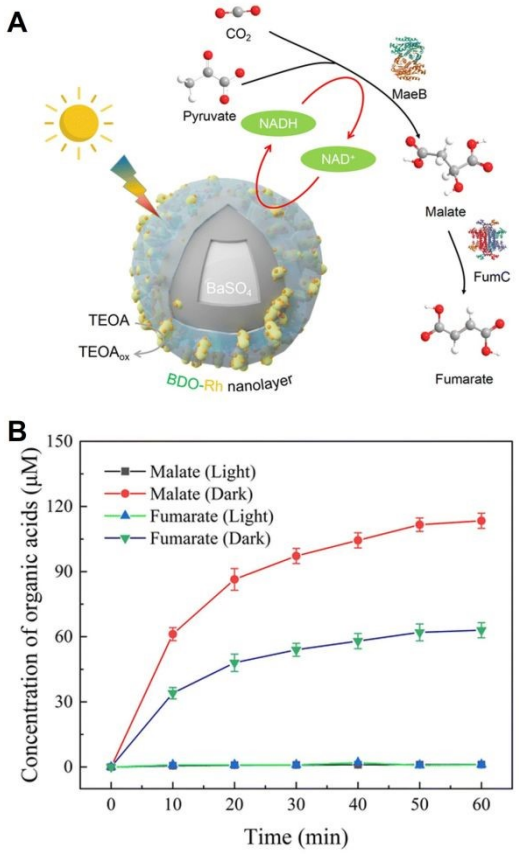

Fig. 52. Schematic representation for visible-light driven fumarate production from pyruvate and CO_2 with the system of TEOA, BaPP@BDO-Rh, NAD^+, MaeB and FumC (A). Time dependence of malate and fumarate production from pyruvate and CO_2 with the system of TEOA, BaPP@BDO-Rh, NAD^+, MaeB and FumC (B). Reproduced with permission from ref 191. Copyright 2023 The Royal Society of Chemistry.

View Article Online
DOI: 10.1039/D5CC00337F

In this study, ME and FUM are expressed in *E. coli strain DE3* using the pET28a vector, and then the enzymes are purified for use in this reaction. The ME and FUM are designated as MaeB and FumC, respectively. The sample solution consists of TEOA (1.0 M), 1 g L^{-1} BaPP@BDO-Rh, NAD^+ (1.0 mM), sodium pyruvate (5.0 mM), sodium bicarbonate (100 mM), magnesium chloride (5.0 mM), MaeB (1.0 U) and FumC (1.0 U) in 3.0 mL of 100mM phosphate buffer. The sample solution is irradiated with 100 W xenon lamp at room temperature as a visible light source. By using this system, the concentration of L-malate and fumarate are estimated to be 114 and 63 μM, respectively after 1 h irradiation as shown in Figure 52(B).

On the other hand, no malate and fumarate production are observed under dark conditions. It is believed that malate production under irradiation and dark in this reference is reversed. Moreover, 79 μM of fumarate is produced using this system after 3 h irradiation. The production of L-malate and fumarate tend to reach a constant concentration during irradiation in this system.

Visible-light driven fumarate production from pyruvate and CO_2 with the system of TEOA, $ZnTMAP^{4+}$, $[RhCp^*(bpy)(H_2O)]^{2+}$, NAD^+, ATP, acetyl-CoA, PC, MDH and FUM has been reported.[184] L-Malate and fumarate production are observed with the system of sodium pyruvate (5.0 mM), acetyl-CoA (1.0 mM), magnesium chloride (5.0 mM), sodium ATP (5.0 mM), TEOA (0.2 M), $ZnTMAP^{4+}$ (50 μM), NAD^+ (5.0 mM), $[RhCp^*(bpy)(H_2O)]^{2+}$ (0.1 mM), PC (1.0 U), MDH (20 U) and FUM (0.5 U) in 5.0 mL of 500 mM HEPES-NaOH buffer solution (pH 7.8) under visible-light irradiation with 250 W Halogen lamp (λ > 390 nm). A balloon filled with 1 L of mixture gas of N_2 and CO_2 is attached to the reaction vessel, and the pressure inside the reaction system is maintained at 1.0 atm. Under condition using a gas mixture containing 15% CO_2, *ca.*213 and 57.6 μM of L-malate and fumarate are produced after 5 h irradiation. Furthermore, no significant difference is observed between L-malate and fumarate production under mixed gas conditions containing 50% CO_2.

On the other hand, it has also been shown that L-malate and fumarate production is reduced by approximately half under mixed gas conditions containing 100%CO_2 or 2% CO_2. By complementing the catalytic function of ME with PC and MDH and using it together with FUM, visible-light driven fumarate production can be achieved using low-concentration CO_2 (approximately 15%) as a direct feedstock.

Finally, an overview of the visible-light driven fumarate production from CO_2 and pyruvate using photocatalytic dye and enzyme hybrid system reviewed in this section is summarized in Table 3.

Major challenges and future trends

Here, the problems and prospects for future demonstration of the systems introduced in this manuscript will be discussed. First, let's discuss the challenges to practical application of visible-light driven plastic precursor production from CO_2 using a photocatalyst and microbial cell hybrid system. The reaction scale of visible-light driven plastic precursor production from CO_2 using a photocatalyst and microbial cell hybrid system will be discussed. As described in the paper, the reaction scale of the hybrid system is approximately 1.0 L at the maximum laboratory level. Scaling up this system for material production involves several significant challenges, including maintaining product quality stability, ensuring process efficiency, and, in some cases, complying with regulatory requirements.

Table 3. Summary of the visible-light driven fumarate production from carbonate species and pyruvate using photocatalytic dye and enzyme hybrid system

System	Fumarate production (μM)	Ref
TEOA (0.2 M), $ZnTPPS^{4-}$ (10 μM), $[RhCp^*(bpy)(H_2O)]^{2+}$ (10 μM), NAD^+ (0.5 mM), sodium pyruvate (5.0 mM), sodium bicarbonate (100 mM), magnesium chloride (5.0 mM), ME (0.7 U) and FUM (0.5 U)	48 (5 h)	177
sodium pyruvate (5.0 mM), TEOA (0.2 M), $ZnTPPS^{4-}$ (10 μM), $[RhCp^*(bpy)(H_2O)]^{2+}$ (10 μM), NAD^+ (0.5 mM), magnesium chloride (5.0 mM), ME (0.7 U) and FUM (0.5 U) in CO_2 saturated buffer	49 (5h)	178
sodium pyruvate (5.0 mM), TEOA (0.2 M), $ZnTMAP^{4+}$ (50 μM), $[RhCp^*(bpy)(H_2O)]^{2+}$ (10 μM), NAD^+ (0.5 mM), magnesium chloride (5.0 mM), ME (0.7 U) and FUM (0.5 U) in CO_2 saturated buffer	97 (5h)	179
TEOA (1.0 M), 1 g L^{-1} BaPP@BDO-Rh, NAD^+ (1.0 mM), sodium pyruvate (5.0 mM), sodium bicarbonate (100 mM), magnesium chloride (5.0 mM), MaeB (1.0 U) and FumC (1.0 U)	63 (1 h)	191
sodium pyruvate (5.0 mM), acetyl-CoA (1.0 mM), magnesium chloride (5.0 mM), sodium ATP (5.0 mM), TEOA (0.2 M), $ZnTMAP^{4+}$ (50 μM), NAD^+ (5.0 mM), $[RhCp^*(bpy)(H_2O)]^{2+}$ (0.1 mM), PC (1.0 U), MDH (20 U) and FUM (0.5 U) in 15%CO_2-saturated buffer	58 (5h)	184

In addition, while Xe and halogen lamps are currently used as visible light sources, it will be necessary to directly utilize solar-light in the future, and the design of the reaction vessel for this purpose will be an important factor. Visible-light driven plastic precursor production from CO_2 using a photocatalyst and microbial cell hybrid system is still under development, and future developments in chemical engineering will likely pave the way for its practical application through the design of the reaction apparatus. On the other hand, hybrid system has the advantage of efficiently promoting CO_2 conversion within microbial cells through induced electrons from solar energy efficiently absorbed using semiconductor photocatalysts and organic dyes. This suggests the potential for more efficient utilization of solar energy compared to CO_2 conversion by photosynthetic microorganisms such as microalgae. In other words, it would be possible to apply a CO_2 conversion apparatus

View Article Online DOI: 10.1039/D5CC03175E

that utilizes the photosynthetic function of microalgae and other organisms, which is already in practical use, to hybrid system.

Visible-light driven plastic precursor production from CO_2 using a photocatalyst and microbial cell hybrid system is attracting attention as an innovative technology that can achieve both the resolution of global challenges and economic growth, but currently, high costs are a major challenge. In particular, this system relies on the growth of microorganisms, resulting in low productivity and increased equipment and purification costs. To overcome these challenges, it is necessary to work on improving large-scale culture technology, advanced separation and purification technology, and the development of bioreactors. Furthermore, the production of high-value-added biodegradable plastics and their precursors from CO_2 will further enhance the value of this system.

Next, let's focus on the direct use of CO_2 gas in hybrid systems. In the visible-light driven plastic precursor production from CO_2 using a photocatalyst and microbial cell hybrid system, a mixed gas with an approximate N_2 to CO_2 ratio of 80:20 is used as the raw material. This is a mixed gas composition optimized for substance production in microbial cells. In some cases, adding hydrogen to a gas mixture can improve the efficiency of producing the desired substance. In particular, in the case of visible-light driven plastic precursor production from CO_2 using a photocatalyst and microbial cell hybrid system, the use of mixed gases, such as exhaust gases emitted from coal-fired power plants, has not yet been considered.

In a visible light-driven biodegradable plastic precursor production system using photocatalytic dyes and multi- enzyme, on the other hand, it is possible to change the composition of the CO_2 gas used as a raw material. In other words, this system has the potential to use CO_2 diluted with N_2, etc., emitted from coal-fired power plants, as a raw material. It has been reported that exhaust gases contain approximately 0.02 to 0.3% NO_x and SO_2.[192] Here, a significant advantage of visible light-driven biodegradable plastic precursor production system using photocatalytic dyes and multi- enzyme is that it allows for the capture of CO_2 gas in the reaction solution using a weakly basic buffer. In addition, because a buffer solution is used, even if NO_x or SO_2 is captured, the pH of the reaction solution will not change, and it is expected that this will not significantly affect the total process.

Finally, let's discuss the hybrid systems introduced in this manuscript from the perspective of life cycle analysis (LCA). There are currently no reported cases of LCA estimation for photocatalysts, biocatalysts, or microbial cell hybrid systems. Therefore, this approach based on reports on life cycle assessments (LCA) for hydrogen production based on water splitting using semiconductor photocatalysts will be discussed.[193] According to this report, in the production of 1 kg of hydrogen using semiconductor photocatalysts, greenhouse gases are mainly released during the preparation of the photocatalyst (95.87%). On the other hand, let's discuss LCA for biocatalytic CO_2 conversion based on bioelectrochemical methods using microbial cell.[194] LCA evaluations of this system estimate that its carbon footprint is comparable to that of fermentation or plant-based manufacturing methods. In other words, it goes without saying that a hybrid system of semiconductor photocatalysts and microbial cells also has the potential to contribute to CO_2 reduction. These conclusions suggest that, at this stage, there are many hurdles to overcome before hybrid systems can achieve significant CO_2 reduction. On the other hand, the fact that value-added substances can be produced from CO_2 and biomass-derived compounds using light energy as a driving force suggests that it would be better to shift the focus from CO_2 reduction to its effective use as a raw material.

Conclusion and outlook

In this review article, focusing on the biodegradable plastics and their precursors production from gaseous CO_2 using the system of visible-light driven redox with biocatalytic processes, the following points are outlined.

1) Visible-light driven production of biodegradable plastic precursors acetate, shikimic acid and acetoin from CO_2 with the hybrid system of inorganic or organic based semiconductor photocatalyst and microbial cell.
2) Visible-light driven production of biodegradable plastic PHB from CO_2 with the hybrid system of inorganic or organic based semiconductor photocatalyst and microbial cell.
3) Visible-light driven production of biodegradable plastic precursor, 3-hydroxybutyrate from acetone and CO_2 with the combination of NAD^+ reduction system of triethanolamine, water-soluble zinc porphyrin, $[Cp^*Rh(bpy)(H_2O)]^{2+}$ and cell extract including dual-enzymes.
4) Visible-light driven production of biodegradable plastic precursors, L-malate fumarate from bio-based pyruvate and CO_2 with the photoredox system of an electron donor, a photosensitizer, an electron mediator and enzyme-based biocatalyst.

In the future, it is expected that innovative technologies with photo/biocatalytic hybrid system will be developed for the effective and practical use for the visible-light driven production of biodegradable plastics and their precursors from gaseous CO_2 and small organic molecules. Therefore, research introduced this article contributes to the CO_2 fixation, and to alternative plastic or its precursor production for sustainable society. These systems can fix gaseous CO_2 in small organic molecules and convert into high-value-added materials, resulting in long-term storage of CO_2 in molecules.

Conflicts of interest

There are no conflicts to declare.

Data Availability Statement

No primary research results have been included, and no new data were generated or analysed as part of this review article.

View Article Online
DOI: 10.1039/D5CC00317F

Acknowledgements

Our work introduced in this review is partially supported by Grant-in-Aid for Specially Promoted Research (23H05404), Scientific Research (B) (25K01584), (23K23140), (22H01872), and (22H01871).

Notes and references

1 G. Q. Chen and M. K. Patel, *Chem. Rev.* 2012, **112**, 2082.
2 R. Kajaste and P. Oinas, *AIMS Environ. Sci.* 2021, **8**, 371.
3 J. Hammer, M. H. Kraak and J. R. Parsons, *Rev. Environ. Contam. Toxicol.* 2012, **220**, 1.
4 T. R. Walker and D. Xanthos, *Resour. Conserv. Recycl.* 2018, **133**, 99.
5 P. Stoett, V. M. Scrich, C. I. Elliff, M. M. Andrade, N. de M. Grilli and A. Turra, *World Development* 2024, **184**, 106756.
6 R. Ciriminna and M. Pagliaro, *ChemistryOpen*, 2020, **9**, 8.
7 Handbook of Bioplastics and Biocomposites Engineering Applications, S. Pilla (Ed.), Wiley-Scrivener, Salem (MA): **2011**.
8 Nova-Institute, Bio-based Building Blocks and Polymers, Hurth (Germany): **2019**.
9 C. Gioia, G. Giacobazzi, M. Vannini, G. Totaro, L. Sisti, M. Colonna, P. Marchese and A. Celli, *ChemSusChem*, 2021, **14**, 4167.
10 L. Filiciotto and G. Rothenberg, *ChemSusChem*, 2021, **14**, 56.
11 T. P. Haider, C. Völker, J. Kramm, K. Landfester and F. R. Wurm, *Angew. Chem. Int. Ed.* 2019, **58**, 50.
12 S. Agarwal, *Macromol. Chem. Phys.,* 2020, **221**, 2000017.
13 A. Ammala, *Prog. Polym. Sci.* 2011, **36**, 1015.
14 A. S. Al Hosni, J. K. Pittman and G. D. Robso, *Waste Manage.* 2019, **97**, 105.
15 T. K. Chua, M. Tseng and M. K. Yang, *AMB Express*, 2013, **3**, 8.
16 L. Cosgrove, P. L. McGeechan, G. D. Robson and P. S. Handley, *Appl. Environ. Microbiol.* 2007, **73**, 5817.
17 M. Karamanlioglu, A. Houlden and G. D. Robson, *Int. Biodeter. Biodegr.* 2014, **95**, 301.
18 V. Nagarajan, A. K. Mohanty and M. Misra, *ACS Sustain. Chem. Eng.* 2016, **4**, 2899.
19 O. Martin and L. Avérous, *Polymer* 2001, **42**, 6209.
20 H. R. Kricheldorf and J. M. Jonté, *Polym. Bull.* 1983, **9**, 276.
21 Y. K. Jung, T. Y. Kim and T. Yong, *Biotechnol. Bioengineer.,* 2009, **105**, 161.
22 S. Bengtsson, A. Werker, M. Christensson and T. Welander, *Bioresour. Technol.,* 2008, **99**, 509.
23 S. Mohapatra, B. Sarkar, D. P. Samantaray, A. Daware, S. Maity, S. Pattnaik, S. Bhattacharjee, *Environ. Technol.* 2017, **38**, 1.
24 S. Bengtsson, A. Werker and T. Welander, *Water Sci. Technol.* 2008, **58**, 323.
25 F. Morgan-Sagastume, A. Karlsson and P. Johansson, S. Pratt, N. Boon, P. Lant and A. Werker, *Water Res.* 2010, **44**, 5196.
26 F. Morgan-Sagastume, M. Hjort, D. Cirne, F. Gérardin, S. Lacroix, G. Gaval, L. Karabegovic, T. Alexandersson, P. Johansson, A. Karlsson, S. Bengtsson, M. V. Arcos-Hernández, P. Magnusson and A. Werker, *Bioresour. Technol.* 2015, **181**, 78.
27 P. Chakravarty, V. Mhaisalkar and T. Chakrabarti, *Bioresour. Technol.,* 2010, **101**, 2896.
28 G. Q. Chen, *Chem. Soc. Rev*., 2009, **38**, 2434.
29 K. Sudesh, H. Abe and Y. Doi, *Prog. Polym. Sci.*, 2000, **25**, 1503.
30 S. Chanprateep, *J. Biosci. Bioeng.,* 2010, **110**, 621.
31 R. Rai, T. Keshavarz, J. A. Roether, A. R. Boccaccini and I. Roy, *Mater. Sci. Eng., R* 2011, **72**, 29.
32 P. K. Samantaray, A. Little, D. M. Haddleton, T. McNally B. Tan, Z. Sun, W. Huang, Y. Ji and C. Wan, *Green Chem.* 2020, **22**, 4055.
33 S. Mohapatra, S. Maity, H. R. Dash, S. Das, S. Pattnaik, C. C. Rath and D. Samantaray, *Biochem. Biophys. Rep*, 2017, **12**, 206.
34 K. Yamane, H. Sato, Y. Ichikawa, K. Sunagawa and Y. Shigaki, *Polym. J.*, 2014, **46**, 76.
35 E. Göktürk, A. G. Pemba and S. A. Miller, *Polym. Chem.*, 2015, **6**, 3918.
36 M. Labet and W. Thielemans, *Chem. Soc. Rev.*, 2009, **38**, 3484.
37 J. O. Iroh, Polymer Data Handbook, J. E. Mark Oxford University Press, New York, 1999, pp. 361–362.
38 H. Bittiger, R. H. Marchessault and W. D. Niegisch, *Acta Crystallogr., Sect. B: Struct. Crystallogr. Cryst. Chem.,* 1970, **26**, 1923.
39 R. A. Gross and B. Kalra, *Science*, 2002, **297**, 803.
40 Y. Ikada and H. Tsuji, *Macromol. Rapid Commun.*, 2000, **21**, 117.
41 T. F. Nelson, R. Baumgartner, M. Jaggi, S. M. Bernasconi, G. Battagliarin, C. Sinkel, A. Künkel, H. P. E. Kohler, K. McNeill1 and M. Sander, *Nat. Commun.* 2022, **13**, 5691.
42 K. S. Savitha, B. R. Paghadar, M. S. Kumar and R. L. Jagadish, *Polym. Chem.*, 2022, **13**, 3562.
43 Y. Doi, K. Kasuya, H. Abe, N. Koyama, I. Shin-ichi, T. Koichi and Y. Yoshida, *Polym. Degrad. Stab.* 1996, **51**, 281.
44 K. Kasuya, K. Takagi, S. Ishiwatari, Y. Yoshida and Y. Doi, *Polym. Degrad. Stab.* 1998, **59**, 327.
45 A. Kilic, E. Yasar, H. İ. Önal, F. Koyuncu, M. Aydemir and F. Durap. *Energy & Fuels* 2025, **39**, 23241.
46 F. Tufano, C. Napolitano, M. Mazzeo, F. Grisi and M. Lamberti, *Biomacromolecules* 2024, **25**, 4523.
47 S. Ye, S. Wang, L. Lin, M. Xiao and Y. Meng, *Adv. Ind. Eng. Polym. Res.* 2019, **2**, 143.
48 Y. Y. Wang, J. W. Fan and D. J. Darensbourg, *Angew. Chem. Int. Ed.* 2015, **54**, 10206.
49 D. Zhang, W. Wang, Z. Wang, D. Song, S. Liu, Y. Chen, X. Ma and L. Xia, *J. CO_2 Util.*2025, 102, 103236.
50 A. Stirbet, D. Lazár, Y. Guo and G. Govindjee, *Ann. Bot.* 2019, **126**, 511.
51 A. N. Tikhonov, W. K. Subczynski, *Cell Biochem. Biophys.* 2018, **77**, 47.
52 K. Asada, *Annu. Rev. Plant Physiol. Plant Mol. Biol*. 1999, **50**, 601.
53 T. Shikanai, *Annu. Rev. Plant Biol.* 2007, **58**, 199.
54 Y. Okegawa, Y. Kagawa, Y. Kobayashi and T. Shikanai, *Plant Cell Physiol.* 2008, **49**, 825.
55 B. V. Trubitsin, A. V. Vershubskii, A. I. Priklonskii and A. N. Tikhonov, *J. Photochem. Photobiol. B*, 2015, **152**, 400.
56 J. Bassham, A. Benson and M. Calvin, *J. Biol. Chem*. 1950, **185**, 781.
57 J. K. Sainis, D. N. Dani and G. K. Dey, *J. Plant Physiol*. 2003, **160**, 23.
58 R. Hidese, M. Matsuda, T. Osanai, T. Hasunuma and A. Kondo, *ACS Synth. Biol.* 2020, **9**, 260.
59 S. Ito, N. Koyama and T. Osanai, *Sci. Rep.* 2019, **9**, 6038.
60 K. Maeda and K. Domen, *J. Phys. Chem. Lett.* 2010, **1**, 2655.
61 S. J. A. Moniz, S. A. Shevlin, D. J. Martin, Z. X. Guoand and J. Tang, *Energy Environ. Sci.* 2015, **8**, 731.
62 K. Takanabe, *ACS Catal.* 2017, **7**, 8006.
63 Y. Wang, H. Suzuki, J. Xie, O. Tomita, D. J. Martin, M. Higashi, D. Kong, R. Abe and J. Tang, *Chem. Rev.* 2018, **118**, 5201.
64 Q. Wang and K. Domen, *Chem. Rev.* 2020, **120**, 919.
65 K. Kaiya, Y. Ueki, H. Kawamoto, K. Watanabe, S. Yoshino, Y. Yamaguchi and A. Kudo, *Chem. Sci.*, 2024, **15**, 16025.
66 R. N. Ivanovsky, Y. I. Fal, I. A. Berg, N. V. Ugolkova, E. N. Krasilnikova, O. I. Keppen, L. M. Zakharchuc and A. M. Zyakun, *Microbiology* 1999, **145**, 1743.
67 H. G. Wood, *FASEB J*, 1990, **5**, 156.
68 M. C. Evans, B. B. Buchanan and D. I. Arnon, *Proc. Natl. Acad. Sci. USA* 1966, **55**, 928.

69 H. Berberoğlu, N. Barra, L. Pilon and J. Jay, *J. Appl. Microbiol.* 2007, **104**, 105.
70 W. Eisenreich, G. Strauss, U. Werz, G. Fuchs and A. Bacher, *Eur. J. Biochem.* 1993, **215**, 619.
71 S. W. Ragsdale, J. E. Clark, L. G. Ljungdahl and H. L. Drake, *J. Biol. Chem.* 1983, **258**, 2364.
72 S. W Ragsdale and E. Pierce, *Biochim. Biophys. Acta* 2008, **1784**, 1873.
73 H. H. Cheng, J. C. Syu, S. Y. Tien and L. M. Whang, *Bioresour. Technol.* 2018, **226**, 229.
74 Y. Xiea, S. Erşanb, X. Guana, J. Wanga, J. Shac, S. Xua, J. A. Wohlschlegelc, J. O. Park and C. Liu, *Proc. Natl. Acad. Sci. USA* 2023, **120**, e2308373120.
75 M. Hermann, A. Teleki, S. Weitz, A. Niess, A. Freund, F. R. Bengelsdorf and R. Takors, *Microb. Biotechnol*. 2020, **13**, 1831.
76 K. K. Sakimoto, A. B. Wong and P. Yang, *Science* 2016, **351**,74.
77 D. P. Cunningham and L. L. Lundie Jr., *Appl. Environ. Microbiol.* 1993, **59**, 7.
78 H. Zhang, H. Liu, Z. Tian, D. Lu, Y.Yu, S. Cestellos-Blanco, K. K. Sakimoto and P. Yang, *Nat. Nanotechnol.* 2018, **13**, 900.
79 K. K. Sakimoto, S. J. Zhang and P. Yang, *Nano Lett.* 2016, **16**, 5883.
80 P. Gai, W. Yu, H. Zhao, R. Qi, F. Li, L. Liu, F. Lv and S. Wang, *Angew. Chem. Int. Ed.* 2020, **59**, 7224.
81 B. Möller, R. Oßmer, B. H. Howard, G. Gottschalk and H. Hippe , *Arch. Microbiol.* 1984, **139**, 388.
82 K. Nevin, T. L. Woodard, A. E. Franks, Z. M. Summers and D. R. Lovley, *mBio.* 2010, **1**, e00103-10.
83 D. R. Lovley and K. P. Nevin, *Curr. Opin. Biotechnol.* 2013, **24**, 385.
84 Y. He, S. Wang, X. Han, J. Shen, Y. Lu, J. Zhao, C. Shen and L. Qiao, *ACS Appl. Mater. Interfaces* 2022, **14**, 23364.
85 Q. Wang, S. Kalathil, C. Pornrungroj, C. D. Sahm and E. Reisner, *Nat. Catal.* 2022, **5**, 633.
86 N. Wen, Q. Jiang and D. Liu, *Sci. Adv.* 2024, **10**, eadp8567.
87 S. Günes, H. Neugebauer and N. S. Sariciftci, *Chem. Rev.* 2007, **107**, 1324.
88 G. Li, V. Shrotriya, J. Huang, Y. Yao, T. Moriarty, K. Emery and Y. Yang, *Nat. Mater.* 2005, **4**, 864.
89 N. Wen, Q. Jiang, J. Cui, H. Zh, B. Ji and D. Liu, *Nano Today* 2022, **47**, 101681.
90 S. Tamang, C. Lincheneau, Y. Hermans, S. Jeong and P. Reiss, *Chem. Mater.* 2016, **28**, 2491.
91 M. Rafipoor, H. Tornatzky, D. Dupont, J. Maultzsch, M. D. Tessier, Z. Hens and H. Lange, *J. Chem. Phys.* 2019, **151**, 154704.
92 M. D. Tessier, D. Dupont, K. De Nolf, J. De Roo, and Z. Hens, *Chem. Mater.* 2015, **27**, 4893.
93 Y. Ding, J. R. Bertram, C. Eckert, R. R. Bommareddy, R. Patel, A. Conradie, S. Bryan and P. Nagpal, *Energy Environ. Sci.* 2019, **141**, 10272.
94 C. Liu, J. J. Gallagher, K. K. Sakimoto, E. M. Nichols, C. J. Chang, M. C. Chang and P. Yang, *Nano Lett.* 2015, **15**, 3634.
95 J. Kim, S. Cestellos-Blanco, Y. X. Shen, R. Cai and P. Yang, *Nano Lett.* 2022, **22**, 5503.
96 S. Cheemanapalli, R. Mopuri, R. Golla, C. M. Anuradha and S. K. Chitta, *Biomed. Pharmacother.* 2018, **108**, 547.
97 J. Guo, M. Suástegui, K. K. Sakimoto, V. M. Moody, G. Xiao, D. G. Nocera and N. S. Joshi, *Science,* 2018, **362**, 813.
98 M. Suástegui, C. Yu Ng, A. Chowdhury, W. Sun, M. Cao, E. House, C. D. Maranas and Z. Shao, *Metab. Eng.* 2017, **42**, 134.
99 R. Hatti-Kaul, U. Törnvall, L. Gustafsson and P. Börjesson, *Trends Biotechnol.* 2007, **25**, 119.
100 Z. Xiao and J. R. Lu, *Biotechnol. Adv.* 2014, **32**, 492.
101 S. Maina, A. A. Prabhu, N. Vivek, A. Vlysidis, A. Koutinas and V. Kumar, *Biotechnol. Adv*. 2022, **54**, 107783.
102 W. Meng, C. Ma, P. Xu and C. Gao, *Trends Biotechnol.* 2022, **40**, 958.
103 Z. Guo, X. Zhao, Y. He, T. Yang, H. Gao, G. Li, F. Chen, M. Sun, J. K. Lee and L. Zhang, *J. Microbiol. Biotechnol.* 2016, **27**, 92.
104 M. Otagiri, S. Ui, Y. Takusagawa, T. Ohtsuki, G. Kurisu and M. Kusunoki, *FEBS Lett.* 2010, **584**, 219.
105 Z. Wang, Q. Song, M. Yu, Y. Wang, B. Xiong, Y. Zhang, J. Zheng and X. Ying, *Appl. Microbiol. Biotechnol.* 2014, **98**, 641.
106 Y. Tian, Z. Guo, J. He, D. Xu, W. W. Li, S. Cheng and H. Song, *J. CO_2 Util.* 2025, **93**, 103051.
107 B. Fu, X. Mao, Y. Park, Z. Zhao, T. Yan, W. Jung, D. H. Francis, W. Li, B. Pian, F. Salimijazi, M. Suri, T. Hanrath, B. Barstow and P. Chen, *Nat. Chem.* 2023, **15**, 1400.
108 J. Ackermann, S. Müller, A. Lösche, T. Bley and W. Babel, *J. Biotechnol.* 1995, **39**, 9.
109 C. R. Hankermeyerand and R. S. Tjeerdema, *Rev. Environ. Contam. Toxicol.* 1991, **159**, 1.
110 R. T. Chan, R. A. Russell, H. Marçal, T. H. Lee, P. J. Holden and L. J. R. Foster, *Biomacromolecules* 2013, **15**, 339.
111 E. Markl, H. Grünbichler and M. Lackner, *Novel Tech. Nut. Food Sci.* 2018, **2**, 1.
112 S. P. Mohandas, L. Balan, N. Lekshmi, S. S. Cubelio, R. Philip and I. S. Bright Singh, *J. Appl. Microbio.* 2017, **122**, 698.
113 A. A. Alarfaj, M. Arshad, E. N. Sholkamy and M. A. Munusamy, *Braz. Arch. Bio. Tech.* 2015, **58**, 781.
114 F. A. P. Tassia, L. J. Marcos, D. B. Watanabe, A. Bonomi, L. K. Quines, W. Schmidell, G. M.F. de Aragao, *Bioch. Eng. J.* 2019, **146**, 97.
115 R. S. Sasidharan, S. G. Bhat and M. Chandrasekaran, *Ann. Microbiol.* 2015, **65**, 455.
116 A. Pohlmann, W. F. Fricke, F. Reinecke, B. Kusian, H. Liesegang, R. Cramm, T. Eitinger, C. Ewering, M. Pötter, E. Schwartz, A. Strittmatter, I. Voss, G. Gottschalk, A. Steinbüchel, B. Friedrich and B. Bowien, *Nat. Biotechnol.* 2006, **24**, 1257.
117 C. Liu, B. C. Colón, M. Ziesack, P. A. Silver and D. G. Nocera, *Science*, 2016, **352**, 1210.
118 M. Xu, P. L. Tremblay, L. Jiang and T. Zhang, *Green Chem.* 2019, **21**, 2392.
119 P. L. Tremblay, M. Xu, Y. Chen and T. Zhang, *iScience*, 2020, 23, 100784.
120 J. Liu, Y. Zhang, L. Lu, G. Wu and W. Chen, *Chem. Commun.* 2012, **48**, 8826.
121 J. Liu, Y. Liu, N. Liu, Y. Han, X. Zhang, H. Huang, Y. Lifshitz, S. T. Lee, J. Zhong and Z. Kang, *Science*, 2015, **347**, 970.
122 P. B. Pati, G. Damas, L. Tian, D. L. A. Fernandes, L. Zhang, I. B. Pehlivan, T. Edvinsson, C. M. Araujo and H. Tian, *Energy Environ. Sci.* 2017, **10**, 1372.
123 W. Yu, M. V. Pavliuk, A. Liu, Y. Zeng, S. Xia, Y. Huang, H. Bai, F. Lv, H. Tian and S. Wang, *ACS Appl. Mater. Interfaces* 2023, **15**, 2183.
124 Z. Sun, J. A. Ramsay, M. Guay and B. A. Ramsay, *Appl. Microbiol. Biotechnol.* 2007, **74**, 69.
125 Y. Li, S. Li, K. Qu, J. Yang, S. Wang and Z. Yan, *J. Environ. Sci.* 2025, **55** DOI: 10.1016/j.jes.2025.07.037.
126 W. Wang, M. Zhang, M. Guo, J. Wang, X. Wang, J. Yin, L. Chen and Y. Li, *Green Chem.* 2026, **28**, 213.
127 Y. Zheng, L. Lin, B. Wang and X. Wang, *Angew. Chem. Int. Ed.* 2015, **54**, 12868.
128 W. Wang, H. Zhang, M. Guo, H. Dong, M. Zhang and L. Chen, *ACS Sustainable Chem. Eng.* 2025, **13**, 7043.
129 Y. Kita, R. Fujii and Y. Amao, *Sustainable Energy Fuels*, 2023, **7**, 360.
130 Y. Kita and Y. Amao, *Catal. Surv. Asia.* 2023, **27**, 67.
131 Y. Kita and Y. Amao, *Chem. Commun.* 2022, **58**, 11131.
132 Y. Kita and Y. Amao, *Green Chem*. 2023, **25**, 2699.
133 C. Rosier, N. Leys, C. Henoumont, M. Mergeay and R. Wattiez, *Applied Microbiol. Biotechnol.* 2012, **78**, 4516.

134 M. K. Sluis, R. A. Larsen, J. G. Krum, R. Anderson, W. W. Metcalf and S. A. Ensign, *J. Bacteriol.* 2002, **184**, 2969.
135 T. Katagiri and Y. Amao, *Green Chem.* 2020, **22**, 6682.
136 Y. Amao, *Sustainable Energy Fuels*, 2018, **2**, 1928
137 Y. Amao, *Chem. Rev.* 2026, DOI: 10.1021/acs.chemrev.5c00754
138 R. Gupta and A. K. Pal, *Sustainable Energy Fuels*, 2024, **8**, 4709.
139 W. Lubitz, H. Ogata, O. Rüdiger and E. Reijerse, *Chem. Rev*. 2014, **114**, 4081.
140 H. Jia, L. Wanb, Y. Gaoc, P. Duc, W. Lic, H. Luoc, J. Ningc, Y. Zhaoc, H. Wangd, L. Zhangd and L Zhang, *J. Energy Chem.* 2023, **85**, 348.
141 S. I. Allakhverdiev, V. D. Kreslavski, V. Thavasi, S. K. Zharmukhamedov, V. V. Klimov, T. Nagata, H. Nishihara and S. Ramakrishna, *Photochem. Photobiol. Sci.* 2009, **8**, 148.
142 Y. Liu, C. Pulignani, S. Webb, S. J. Cobb, S. Rodríguez-Jiménez, D. Kim, R. D. Milton and E. Reisner, *Chem. Sci.* 2024, **15**, 6088.
143 K. P. Sokol, W. E. Robinson, J. Warnan, N. Kornienko, M. M. Nowaczyk, A. Ruff, J. Z. Zhang and E. Reisner, *Nature Energy* 2018, **3**, 944.
144 C. A. Caputo, L. Wang, R. Beranek and E. Reisner, *Chem. Sci.* 2015, **6**, 5690.
145 K. A. Brown, S. Dayal, X. Ai, G. Rumbles and P. W. King, *J. Am. Chem. Soc.* 2010, **13**, 9672.
146 K. W. Brown, M. B. Wilker, M. Boehm, G. Dukovic and P. W. King, *J. Am. Chem. Soc.* 2012, **134**, 5627.
147 M. B. Wilker, K. E. Shinopoulos, K. A. Brown, D. W. Mulder, P. W. King and G. Dukovic,. *J. Am. Chem. Soc.* 2014, **136**, 4316.
148 Y. Honda, H. Hagiwara, S. Ida and T. Ishihara, *Angew. Chem., Int. Ed.* 2016, **55**, 8045.
149 Y. Honda, Y. Shinohara and H. Fujii, *Catal. Sci. Technol.* 2020, **10**, 6006.
150 Y. Honda, M. Yamamoto, Y. Shinohara, Y. Hatanaka, M. Watanabe, T. Ishihara and H. Fujii, *ACS Appl. Nano Mater.* 2025, **8**, 21294.
151 Y. Amao, *J. CO_2 Util.* 2018, **26**, 623.
152 M. Moon, G. W. Park, J. Lee, J. S. Lee and K. Min, *J. CO_2 Util.* 2020, **42**, 101353.
153 W. Ma, Q. Geng, C. Chen, Y. C. Zheng, H. L. Yu and J. H. Xu, *ChemBioChem* 2023, **24**, e202300390.
154 A. Maier, L. M. Mguni, A. C. R. Ngo and D. Tischler, *ChemCatChem* 2024, **16**, e202401021.
155 X. Guo, X. Wang, Y. Liu, Q. Li, J. Wang, W. Liu and Z. K. Zhao, *Chem. Eur. J.* 2020, **26**, 16611.
156 D. Mandler and I. Willner, *J. Chem. Soc., Perkin Trans. 2* **198**, 997.
157 X. Huang, L. Xu, H. Qian, X. Wang and Z. Tao, *J. Nanobiotechnol.* 2022, **20**, 295.
158 Z. Chi, G. L. Liu, C. G. Liu and Z. M. Chi, *Applied Microbiol. Biotechnol.* 2016, **10**, 841.
159 C. M. Krell and D. Seebach, *Eur. J. Org. Chem.* 2000, **2000**, 1207.
160 K. Tabata, K. Kasuya, H. Abe, K. Masuda and Y. Doi, *Appl. Environ. Microbiol.* 1999, **65**, 4268.
161 H. Adelnia, H. D. N. Tran, P. J. Little, I. Blakey and H. T. Ta, *ACS Biomater. Sci. Eng.* 2021, 7, 2083.
162 J. J. Pueyo and C. Gömez-Moreno, *Enzyme Microb. Technol.* 1992, **14**, 8.
163 M. T. Bes, A. L. de Lacey, V. M. Fernandez and C. Gömez-Moreno, *Bioelectrochem. Bioenerg.* 1995, **38**, 179.
164 Y. Kim, K. Ikebukuro, H. Muguruma and I. Karube, *J. Biotechnol.* 1998, **59**, 213.
165 H. Inoue, M. Yamachika and H. Yoneyama, *J. Chem. Soc., Faraday Trans.* 1992, **88**, 2215.
166 K. A. Brown, M. B. Wilker, M. Boehm, H. Hamby, G. Dukovic and P. W. King, *ACS Catal.* 2016, **6**, 2201.
167 T. Itoh, H. Asada, K. Tobioka, Y. Kodera, A. Matsushima, M. Hiroto, H. Nishimura, T. Kamachi, I. Okura and Y. Inada, *Bioconjugate Chem.* 2000, **11**, 8.
168 Z. Jiang, C. Lüa and H. Wu, *Ind. Eng. Chem. Res.* 2005, **44**, 4165.
169 Q. Shi, D. Yang, Z. Jiang and J. Li, *J. Mol. Catal. B.* 2006, **43**, 44.
170 S. H. Lee, D. H. Nam, J. H. Kim, J. O. Baeg and C. B. Park, *ChemBioChem* 2009, **10**, 1621.
171 J. H. Kim, S. H. Lee, J. S. Lee, M. Lee and C. B. Park, *Chem. Commun.* 2011, **47**, 10227.
172 Y. Katagiri and Y. Amao, *Sustainable Energy Fuels*, 2022, **6**, 2581.
173 D. H. Nam and C. B. Park, *ChemBioChem* 2012, **13**, 1278.
174 G. Zhao, C. Yang, W. Meng and X. Huang, *J. Mater. Chem. A*, 2024, **12**, 3209.
175 H. Wu, C. Tian, X. Song, C. Liu, D. Yang and Z. Jiang, *Green Chem*. 2013, **15**, 1773.
176 Y. Amao and M. Ishikawa, *Catal. Commun.* 2007, **8**, 523.
177 M. Takeuchi and Y. Amao, *Sustainable Energy Fuels*, 2023, **7**, 355.
178 M. Takeuchi and Y. Amao, *RSC Sustain.* 2023, **1**, 1874.
179 M. Takeuchi and Y. Amao, *Dalton Trans.* 2024, **53**, 418.
180 P. H. Wang, K. Correia, H. C. Ho, N. Venayak, K. Nemr, R. Flick, R. Mahadevan, and E. A. Edwards, *ISME J.* 2019, **13**, 1042.
181 M. J. MacDonald, *J. Biol. Chem.* 1995, **270**, 20051.
182 M. Takeuchi and Y. Amao, *RSC Sustain.* 2024, **2**, 2491.
183 M. Takeuchi and Y. Amao, *New J. Chem.* 2024, **48**, 18055.
184 A. Horikawa and Y. Amao, *Energy & Fuels* 2025, **39**, 19537.
185 M. Takeuchi and Y. Amao, *RSC Sustain.* 2023, **1**, 90.
186 M. Takeuchi and Y. Amao, *New J. Chem.* 2023, **47**, 17679.
187 I. A. Rose, J. V. B. Warms and D. J. Kuo, *Biochemistry* 1992, **31,** 9993.
188 I. A. Rose, J. V. B. Warms and R. G. Yuan, *Biochemistry* 1993, **32,** 8504.
189 S. Beeckmans and E. van Driessche, *J. Biol. Chem.* 1998, **273**, 31661.
190 M. Takeuchi and Y. Amao, *J. Jpn. Petrol. Inst.* 2024, **67**, 167.
191 G. Li, Z. Lin, X. Li, Y. Zhang, W. Zhu, Y. Shao, Q. Xue, Q. Fan, T. Tan and H. Cao, *J. Mater. Chem. A,* 2024, **12**, 192.
192 S. K. Guttikunda and P. Jawahar, *Atmos. Environ.* 2014, **92**, 449.
193 V. B. Y. Oh, S. F. Ng and W. J. Ong, *J. Clean. Prod.* 2022, **379**, 134673.
194 S. Das, S. Das, M. M. Ghangrekar and B. Min, *J. Environ. Chem. Eng.* 2025, **13**, 119221.

View Article Online
DOI: 10.1039/D6CC00317F

Data Availability Statement

No primary research results have been included and no new data were generated or analysed as part of this review article.